Modelling Neurons and Their Collective Behaviour

Saurabh Bedi
Roll No: MS15095

A dissertation submitted for the partial fulfillment
of BS-MS dual degree in Science

Under the guidence of
Dr. Satyajit Jena and Prof. Somdatta Sinha

Indian Institute of Science Education and Research Mohali

May 2020

Certificate of Examination

This is to certify that the dissertation titled **" Modelling Neurons and Their Collective Behaviour"** submitted by Mr. **Saurabh Bedi** (Reg. No. MS15095) for the partial fulfilment of BS-MS dual degree programme of the Institute, has been examined by the thesis committee duly appointed by the Institute. The committee finds the work done by the candidate satisfactory and recommends that the report be accepted.

Dr. Abhishek Chaudhari Dr. Rajeev Kapri Dr. Satyajit Jena
(Supervisor)

Prof. Somdatta Sinha
(Co-Supervisor)

Dated: 27.05.2020

Declaration

The work presented in this dissertation has been carried out by me under the guidance of Dr. Satyajit Jena and Prof. Somdatta Sinha at the Indian Institute of Science Education and Research, Mohali.

This work has not been submitted in part or in full for a degree, a diploma, or a fellowship to any other university or institute. Whenever contributions of others are involved, every effort is made to indicate this clearly, with due acknowledgement of collaborative research and discussions. This thesis is a bonafide record of original work done by me and all sources listed within have been detailed in the bibliography.

Saurabh Bedi
(Candidate)

Dated: May 27, 2020

In my capacity as the supervisor of the candidate's project work, I certify that the above statements by the candidate are true to the best of my knowledge.

Dr. Satyajit Jena
(Thesis supervisor)

In my capacity as the co-supervisor of the candidate's project work, I certify that the above statements by the candidate are true to the best of my knowledge.

Prof. Somdatta Sinha
(Thesis co-supervisor)

Acknowledgment

First and foremost, I would like to thank my thesis supervisor Dr. Satyajit Jena, and my thesis co-supervisor Prof. Somdatta Sinha. I started my thesis work under Prof. Somdatta Sinha's guidance, working on the aspects of computational modelling in the thesis. Her mentorship has helped me become a better researcher. Discussions in lab meetings every week were extremely fruitful, and she constantly guided me to become a more careful and meticulous student. Working under her guidance has helped me in gaining a more scientific outlook and in diversifying my knowledge. I cannot thank her enough for the help that she has provided me throughout. I am indebted to Prof. Sinha for her critical edits in the thesis and for providing invaluable insights to make it coherent and precise. I express my sincere gratitude to her for helping me out even amidst such trying circumstances of COVID-19 and the deadly Amphan supercyclone. I am also grateful to Dr. Satyajit Jena for being my supervisor and for guiding me in the second half of my thesis work. He was always available for clarification of doubts and for discussions regarding work. I am amazed at Dr. Jena's commitment to his work and his enthusiasm towards scientific research. I am thankful to him for sharing his keen ideas and for being a source of constant inspiration and motivation. He has been supportive throughout, and he always guided me to sources to improve my skill set and in learning about the theory and techniques in data analysis. It was a wonderful opportunity working under Prof. Somdatta's and Dr. Jena's guidance. I admire the effort and the hard work with which they work, and I wish to imbibe such qualities.

I am also really grateful to the rest of the committee members: Dr. Abhishek Chaudhari and Dr. Rajeev Kapri. Their comments during the poster presentation were very insightful. I incorporated some work motivated by the inputs that they gave me in the thesis as well, and I thank them for their inputs and for always being available to talk to whenever I needed.

My lab members were extremely supportive, and this project would not be so fun and fruitful without their support. I would like to thank Himanshu for discussing bugs in the codes with me, along with being a dear friend. I would also like to thank Inayat and Hayman. They made the experience memorable, and the coffee breaks with the Sinha lab will always be a cherish-able memory. I had a similarly fascinating time at the HPEC lab, and I would like to thank Debanjan and Rohit for being so helping and forthcoming with their discussions related to the coding and the algorithms. I enjoyed having conversations related to topics in neuroscience with Sveekruth. I also express my gratitude to Innovation in Science Pursuit for Inspired Research (INSPIRE) Scholarship of the Department of Science and Technology (DST), and the Indian Institute of Science Education and Research, Mohali (IISERM) for providing financial, and educational support.

I have made friends for life here, and I had some of the best memories with them. I am grateful to Amit for being there for his constant support, Ayush for making last-minute trips to eat, Bhavya for being a caring friend, Rajesh for being there as my late-night study partner, Raju for giving invaluable advice on issues, Rohit for always being there when I needed him, Sahil for managing and distributing the groceries and Surendra for making the most tense moments pleasurable. These people made hostel rooms feel like home. I owe a lot of good memories to Apoorv, Gouri, Megha, and Preeti, without whom my stay here would not be complete. I also owe my sincere gratitude to Shubham for being my study partner and friend through the course of these five years.

I dedicate this work to my parents. I will always be indebted to them, and I cannot thank them enough for their constant support, faith, and encouragement. I also thank my sister Supriya for being a friend and a happy influence on my life.

Saurabh Bedi

MS15095

IISER Mohali.

List of Figures

Contents

Abstract

Electrical activity of a neuron is regulated by the unequal distribution of several ions across its membrane. The standard biophysical model of a neuron was given by Hodgkin and Huxley (HH), who used coupled differential equations involving the differential conductances of the Sodium and Potassium ion channels and the input current as parameters. The model correctly describes the typical voltage impulse dynamics (Action Potential) across the neuronal membrane. This work probes various dynamic behaviour of single neurons at different parameter values through their long-term time course, different features of oscillatory behaviour, and parameter space search for transition in stability that takes place upon changing these parameters. Subsequently, the dynamics of two HH neurons is studied that share membrane voltages through gap junction coupling, for both unidirectional and bidirectional coupling. The dynamic behaviour is then probed for increased number of neurons for different boundary conditions, coupling types, and strengths of coupling. The two boundary conditions probed are - the ring (periodic boundary conditions) and the chain (fixed boundary conditions) of neurons, with bidirectional coupling implemented in the ring, and unidirectional coupling in the chain. The collective behaviour of these networks of neurons is studied for different coupling strengths and input currents. Synchronization in these neuronal networks is studied through Synchronization Order Parameter and Space Time plots. Preliminary studies on a reverse approach of estimating parameter values from neuronal voltage data are also reported. The results obtained in this work are discussed from a nonlinear dynamical systems view.

Chapter 1

Introduction

1.1 Neuron as a dynamical system

Neurons exhibit different types of potentials with time and can change their ion channel properties depending on various physio-chemical and physiological stimuli [1]. Thus, neurons can be considered as dynamical systems. The dynamic behaviour of the action potential generated by a neuron depends on its various ionic properties at that given time. Many mathematical models exist which deal with capturing this complex behaviour of neuronal systems [2]. The complex dynamical behaviour of the neuron are replicated by nonlinear models of coupled differential equations. The models are capable of exhibiting a vast range of dynamics in both single and coupled neurons [2]. First, the biological properties of a typical neuron to explain the origin of the Action Potential have been explained down below. Then, a few significant mathematical models in the field of Computational Neuroscience with the advantages and limitations that exist for each model are discussed.

1.2 Functioning of the biological neuron

A neuron is a type of excitable cell which carries information as electrical signals throughout the body. It has a neuronal membrane which separates ions across it. There is a gradient of ions across this neuronal membrane with a higher concentration of potassium ions inside the neuron and a higher concentration of sodium ions outside the neuron. There are other ions like the Chloride ions etc. which are mostly referred to collectively as the leak ions. In resting state conditions, there exists an electrical gradient across the neuronal membrane,

which renders a potential difference of approximately -70mV to the neuron. The **resting potential** in the neuron is maintained by the Sodium and Potassium pumps. Upon receiving a signal from outside the neuron, the potential difference across the neuron changes, and if it exceeds a particular level of threshold potential, then we get an **action potential**. If it does not cross the threshold, we get a failed initialization called **graded potential**. An action potential is an all or none mechanism, in which either the action potential is completely generated or it is not generated at all. An action potential is essentially a **depolarization** followed by a **repolarization** and subsequently a **hyperpolarization phase**. The depolarization phase occurs due to a rush of sodium ions into the neuron. Eventually, at around 30mV, the Sodium channel closes, and potassium channel opens, forcing Potassium ions to move out and thus start the repolarization phase. There is an overshoot due to the slow closing of the Potassium ion channels, which results in the hyperpolarization phase. This dynamics of action potential generation has been modelled with the help of various mathematical models, and we will look at a few of these down below.

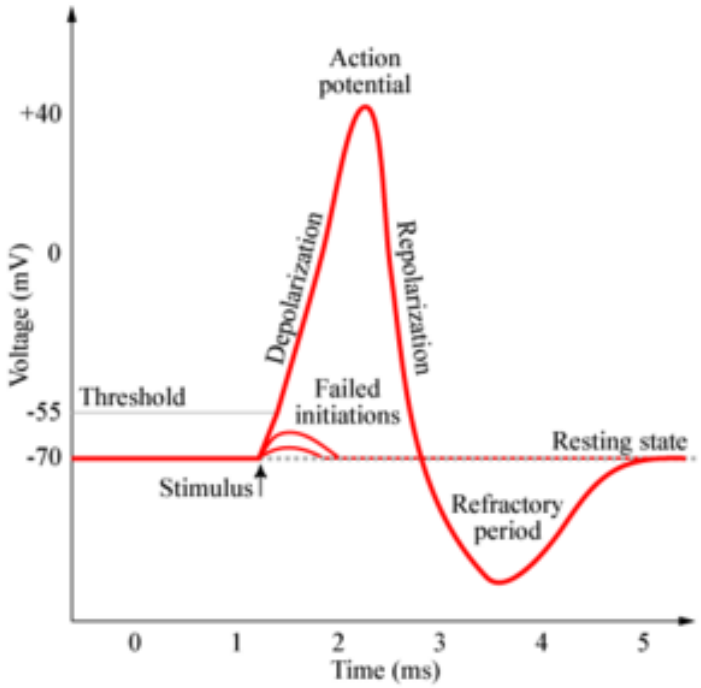

Figure 1.1: Components of an action potential (Figure 1.1 reproduced from $http : //biogeonerd.blogspot.com/2012/02/action - potentials - what - make - your - brain.html$)

1.3 Mathematical models of a single neuron

We discussed that the functions of a biological neuron could be modelled with nonlinear equations. Several models already exist which recreate the behaviour of a neuron. We are mostly interested in models of the electrical input - output membrane Voltage type. As the name suggests, these models take input as current and give voltage as output. There often exists a trade-off between the computational tractability of these models and their ability to simulate real observed biological neural activity. Thus, different models are useful in different contexts. Simpler models might be useful while creating extensive networks requiring higher computational power, while more detailed models would be useful for looking at smaller networks or single neurons at a higher resolution. Below are some of the models which exist in literature.

- Hodgkin Huxley model [3] - It is a very detailed and computationally extensive model of a single neuron and was one of the first mathematical models given. It replicates almost all the features of neuronal excitability and is defined by four state variables (four-dimensional state space).

- Hindmarsh Rose model [4] - A slight simplification of the Hodgkin Huxley model. This model has a three-dimensional state space. One of the slow variables in the Hodgkin Huxley model is approximated to its asymptotic value [5]. It is unique because it replicates the bursting action potential behaviour that is shown in some excitable cells.

- Fitzhugh Nagumo model [6, 7] - This model is a further simplification and only consists of a two-dimensional state space. This model is obtained by further simplifications by first approximating the slow state variable (m) to its asymptotic value, thus giving up accuracy at the short time scale [5] and by introducing an auxiliary variable that lets us go of another variable.

- Leaky integrate and fire model [8] - This model comes at the opposite end of the spectrum and is the least comprehensive and with the most approximations. It is useful if very large networks are to be constructed, and one can let go of a few features of the biological neuron for simplicity. It is not able to replicate a number of features,

including for example, the refractory period in action potential generation of a real biological neuron.

In this study, the Hodgkin Huxley model has been used which is described in detail in the methods section (Chapter 2).

1.4 Definitions and Theory

The basic theoretical foundation that is used in our study on the dynamic behaviour of Hodgkin Huxley neurons is given down below.

- **Nonlinear systems** are systems whose output does not change linearly with the input and thus, these systems display extreme sensitivity to their initial conditions. Such a system is usually represented mathematically in terms of a set of nonlinear differential equations which are often coupled. These co-ordinates of the output variables of a non linear system collectively represent the **Phase space** of the system. Similarly, the possible co-ordinates of the parameters collectively make up the **parameter space** of the system. Looking at the phase space and the parameter space is useful in making important inferences about the properties of the nonlinear system. An important concept when dealing with nonlinear systems is the concept of **transience**. It is defined as a short period in time when the qualitative behaviour of the system is different from the qualitative behaviour of the system at other times. A transient is usually observed in one of the state space variables in the very beginning, and as time passes, the system reaches its natural state for the given parameters known as the **attractor** of the system [9]. All the initial conditions which make the system end up at the same attractor state are collectively called the **basin of attraction**. The two major types of attractors that are probed in this work, are the fixed point attractor and the periodic/oscillating attractor. An interesting phenomenon that is frequently encountered upon tracking the long term time course of these non linear dynamical systems is the phenomenon of **Bifurcations** [10]. These are phenomenon in which a small change in the input parameters dramatically changes the qualitative behaviour (type of attractor) of the system. Thus, a bifurcation is usually accompanied with a change in the properties of equilibrium and stability of the system.

- **Synchronization** is a broad concept that can be understood as the tuning of rhythms of oscillators due to cross-talk between them. It is one of the most important emergent phenomenon arising in coupled systems [11]. The cross-talk/interaction between these oscillators is a result of **coupling** between the oscillators. The coupling could be weak or strong, depending on the effect of oscillators on each other. Synchronization could be of different types. Two time series that are identical to each other are said to be in **Total/ Complete Synchronization** [12–14]. Total Synchronization/ Complete Synchronization is the strongest type of synchronization. A slightly less strong synchronization type is the **Lag Synchronization**. In lag synchronization, the coupled bodies are synchronized with a lag between them [14]. **Phase Synchronization** is a less strict term in which the coupled bodies remain mostly uncorrelated, however, the time period of the bodies' oscillations are equivalent [14–16]. Essentially, in phase synchronization, the amplitude is largely uncorrelated but the phase difference between time series remains same. Phase Synchronization is a very weak type of synchronization. The amplitude of the two time series could be different in phase synchronization. The difference in phase between the two time series is called **Phase Lagging**. Another concept in synchronization is the concept of **Frequency Matching**. It is the phenomenon of tuning/matching of the frequencies of multiple coupled oscillators. Meanwhile, having no relationship between the frequency spectrum of variables is referred to as **Asynchronization**.

1.5 Importance and Motivation

This section highlights the importance and motivation for the following work. Additionally, a few interesting related pieces of literature are highlighted in the following points.

- Specifically modelling single neurons and small neuronal networks based on circuits found in lower level organisms has helped in understanding specific behavioural responses in these simple organisms. Several pieces of literature probe these behaviours through modelling of the nervous system of these lower level organisms. Examples of this are in modelling the part of the nervous system responsible for different cognitive functions in the Jellyfish [17]. There are plenty of other examples of previous studies which use dynamic models to understand the neural basis of behaviour [18].

- Apart from modelling specific nervous systems and recreating these simple behaviours of lower level organisms, simple general models of the single neuron and their collection can be extremely useful in understanding the general properties of the neuron and the synapse. The underlying dynamic principles which govern neuronal circuits remain the same. Thus, modelling is essential to get a better understanding of the general properties of the neuron and its collection besides looking at specific functions of neuronal networks in certain organisms.

- Rhythmic activity of the brain is essential for various cognitive functions to take place. The brain exhibits this large scale rhythmic behaviour which is captured through techniques like the EEG and the MEG. This rhythmic activity visible globally in the brain or in certain parts of the brain is a result of the synchronization of neuronal networks. Alpha and Gamma EEG rhythms are a result of partial synchrony in cortical brain areas. Excessive synchronization in brain regions could lead to seizures and epilepsy. Thus, understanding the synchronization of brain networks is of primary importance [19].

- The role of the electrical coupling in order to drive synchronization has been comparatively less studied. Instantaneous synchronization is needed in fight or flight responses of organisms living in dangerous environments. Electrical coupling being faster than chemical coupling enables signals to travel faster. This is particularly true for smaller organisms like in rats to speed motor responses [20]. Comparatively less has been studied about the role of the electrical synapse/ gap junction coupling in synchronization, and modelling can help gain insights into this.

1.6 Organization of the thesis

This work studies the dynamic behaviour of single and coupled neurons at different parameter values. Chapter 2 deals with the HH model of the single neuron and an introduction to methods of coupling neurons through gap junction coupling. The method used to map the single neuron parameter space is discussed, and then the chapter ends with discussion on measuring synchronization in multiple coupled neurons. These methods and models discussed in Chapter 2 are then used for probing the dynamic behaviour of single and coupled

neurons, and the results obtained by them are discussed in the following chapters. Chapter 3 deals with the results for the effect of different parameters on the dynamics of the single neuron. Chapter 4 deals with results obtained in two neurons coupled through gap junction coupling, and chapter 5 discusses results for multiple coupled neurons and how changing the number of neurons (along with other parameters) affects synchronization. Chapter 6 deals with methods to simulate noisy data and subsequently the theory of parameter estimation in this noisy data using Bayesian inference. This would link the modelling and the data analysis together. Finally, chapter 7 contains further discussions on results and conclusions.

Chapter 2

Models and Methods

In this study, our focus is on understanding the dynamics of single neurons and small networks of electrically coupled neurons. As discussed in section 1.3, the Hodgkin Huxley model is a really detailed and computationally extensive model and it enables one to replicate most of the features of neuronal excitability shown in a biological neuron. Thus, the HH model is particularly useful in modelling smaller networks of neurons and so we have used it for our purposes. A detailed background on the Hodgkin Huxley model is given in section 2.1 down below.

2.1 The Hodgkin Huxley Model

Hodgkin and Huxley gave the first comprehensive mathematical model which replicated the results and data that they had obtained on the giant squid neuron in a series of papers prior to that [3]. The primary aim of these mathematical models is to replicate the functioning of the neuron and be able to generate action potentials properly in a biological context. Hodgkin and Huxley treated the neuron as a circuit with different parts of the circuit representing different parts of the neuron. The cell membrane was represented by a capacitor (C_m), the electrochemical gradients (V_{Na}, V_l, V_K) were represented as electrochemical batteries supplying a potential difference (V_m) across the capacitor and the signal to the cell was modelled as an external input current (I) given to the circuit. The ion channels are modelled as resistors of variable conductance as their conductance (g_{Na}, g_K, g_l) is a function of time and potential difference. The schematic for the circuit is given in Figure 2.1.

The following are the equations for the model:-

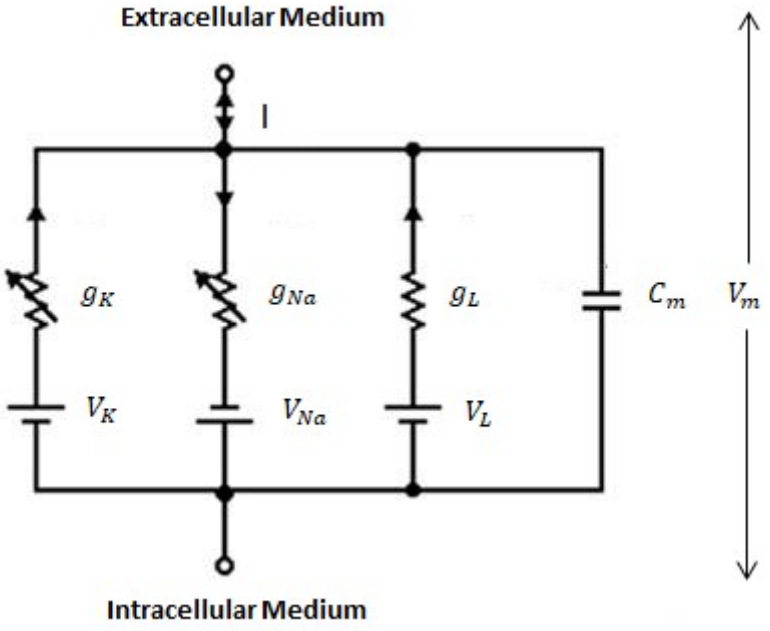

Figure 2.1: The equivalent circuit for Hodgkin Huxley model of the neuron

1. $C_m \frac{dV_m}{dt} = I - g_l(V_m - V_l) - \bar{g}_{Na} m^3 h(V_m - V_{Na}) - \bar{g}_K n^4 (V_m - V_K)$
2. $\frac{dn}{dt} = \alpha_n(V_m)(1-n) - \beta_n(V_m)n$
3. $\frac{dm}{dt} = \alpha_m(V_m)(1-m) - \beta_m(V_m)m$
4. $\frac{dh}{dt} = \alpha_h(V_m)(1-h) - \beta_h(V_m)h$
5. $\alpha_m = 0.1 \frac{(V_m+35.0)}{1-e^{(-\frac{(V_m+35.0)}{10.0}}}$
6. $\beta_m = 4.0e^{(} - \frac{(V_m+60.0)}{18.0}$
7. $\alpha_h = 0.07e^{(} - \frac{(V_m+60.0)}{20.0}$
8. $\beta_h = \frac{1}{1+e^{\frac{(-V_m+30.0)}{10.0}}}$
9. $\alpha_n = 0.01 \frac{V_m+50.0}{1-e^{(-\frac{(V_m+50.0)}{10.0}}}$
10. $\beta_n = 0.125e^{\frac{(-V_m+60.0)}{80.0}}$

These equations mathematically describe the Hodgkin Huxley model of a neuron. The first equation is just the Kirchhoff's law applied on the circuit. Equations 2 to 4 describe the

opening and closing of gates of the ion channels. Equations 5 to 10 describe the values of constants used in the first four equations. These were obtained by Hodgkin and Huxley by analytically fitting a curve to the data. The first four equations describe the dynamics of the state variables (V_m, m, n, and h). The standard values taken for the constants are as follows [3]:-

The capacitance value, $C_m = 1.0\ \mu V$, The reversal potential for Sodium for substituting in our first equation is, $V_{Na} = 115.0\ mV$, reversal potential for Potassium, $V_K = -12.0\ mV$, reversal potential for leak ions is $V_l = 10.613\ mV$. The value for leak conductance, $G_l = 0.3\ \frac{mS}{cm^2}$.

Note that in the original paper, Hodgkin and Huxley worked on the giant squid neuron, and thus, the maximal Potassium and Sodium Conductance were also taken as their standard values. Maximal Sodium Conductance ($\bar{g}_{Na}$) is taken as 120.0 $\frac{mS}{cm^2}$ and maximal Potassium conductance ($\bar{g}_K$) is taken as 36.0 $\frac{mS}{cm^2}$ in the Hodgkin Huxley paper. However, we take these two maximal conductances as variable parameters and see their effects on our model's output voltage (V_m).

Note that the n-gate (second equation) controls the dynamics of the Potassium channel. The m-gate (third equation) and the h-gate (fourth equation) control the dynamics of the Sodium channel. We now look at the dynamics of Sodium and Potassium gated channels individually.

- Sodium Channel - The dynamics of the Sodium gated channel are governed by the m-gate and the h-gate. The dynamics, in fact, depends on the product of powers of m and h. This means that if either of the gates, m-gate or the h-gate are shut, the Sodium channel will remain shut. The h gate is open in the resting state. However, the m-gate is shut. This renders the Sodium gated channel, the off configuration for the resting state of the neuron. When the neuron gets depolarised, the m-gates start opening up rapidly. This opens up the Sodium gated channels. This is known as the **open/ activated configuration** for the Sodium channel. Subsequently, the channel goes into the **inactivated state** as the h-gate shuts. The shutting of the h-gate starts even before repolarization has started. Subsequently, the m-gates also shut in the repolarization phase. There is an **absolute refractory period**, which exists because the h-gate remains shut even if the neuronal membrane is depolarized in this period.

- Potassium channel - The dynamics of the potassium channel is controlled with the

n-gate. Its dynamics are slower than the dynamics of the Sodium gates. Upon depolarization, n-gates slowly open and they slowly close upon repolarization. This gives a slow dynamics to the Sodium Channel.

The collective work of these gates, and the above given equations govern the dynamics of a neuron.

2.2 Modelling of coupled neurons

This study includes work on neurons connected to each other with the help of electrical synapses along with analysis of single neuron dynamics. Gap junction coupling is the most common way in which electrical synapses couple multiple neurons. The first evidence of current flow between cells dates back to around the 1950s [21]. Since then we also know about their presence in brains of mammals [22]. Gap junctions work because they connect the inner portions of nearby cells through many channels. Electrical current and other very small molecules pass through this gap junction. Some gap junctions, however, allow the passage of larger ions as well. They are very useful for synchronizing the electrical activity of the neurons.

There are certain properties that are followed by the transmission of signal via gap junction coupling. Firstly, there is a delay in the signal at the postsynaptic neuron [23]. Also, it is to be noted that electrical synapses transmit information significantly faster than their counterpart chemical synapses, especially in cold blooded animals. Thus these synapses are extremely useful in cold blooded animals requiring a quick motor response. In hot blooded mammals, however, the speed of chemical transmission is really fast as well.

The equations for the single Hodgkin Huxley neuron given in the previous section get changed by the introduction of electrical coupling between neurons. In the first equation, we have the currents due to the Sodium ions, the Potassium ions, and the leak ions that govern the dynamics of the potential difference across the capacitance (cell membrane). All these are referred to as ionic currents (I_{ionic}). As can be clearly seen, the first equation comes from Kirchhoff's laws and describes the total current flowing across the capacitor. As we have an additional current due to the electrical synapse, this equation changes to in-

clude that term. Note that all the other equations except the first equation remain unchanged upon introducing the electrical synapse. This is because the other equations describe the inner workings of a single neuron, and those remain unchanged due to the gap junction coupling. The new set of equations which govern a neuron coupled with an electrical synapse are given by

1. $C_m \frac{dV_m}{dt} = I - I_{ionic} - I_{electrical}$
2. $\frac{dn}{dt} = \alpha_n(V_m)(1-n) - \beta_n(V_m)n$
3. $\frac{dm}{dt} = \alpha_m(V_m)(1-m) - \beta_m(V_m)m$
4. $\frac{dh}{dt} = \alpha_h(V_m)(1-h) - \beta_h(V_m)h$

I_{ionic} refers to current due to all ions, and $I_{electrical}$ refers to the current due to the electrical synapse.

Using a similar analogy of neuronal systems being treated as an electrical circuit taken by the Hodgkin Huxley model, we define the current due to gap junction coupling, $I_{electrical}$ as a product of the conductance value between the two neurons and the Voltage difference between the two neurons ($g_C(V - V_{adjacent})$). Here, $V_{adjacent}$ is the voltage of neurons that affect the neuron we are modelling through electrical coupling. There are two types of coupling that we probe in this work. They are the unidirectional coupling and the bidirectional coupling. A schematic representation of the two types of coupling is given in Figure 2.2. The blue arrows denote the direction of coupling. Further details and equations governing the dynamics for the coupled neurons are given in Chapter 4 (two coupled neurons) and 5 (multiple coupled neurons).

2.3 Methods used to assess the dynamic behaviour of single and coupled neurons

In this section, we give a brief introduction and cite literature on the qualitative and quantitative methods used for parameter analysis in single neurons and for studying synchronization in coupled neurons.

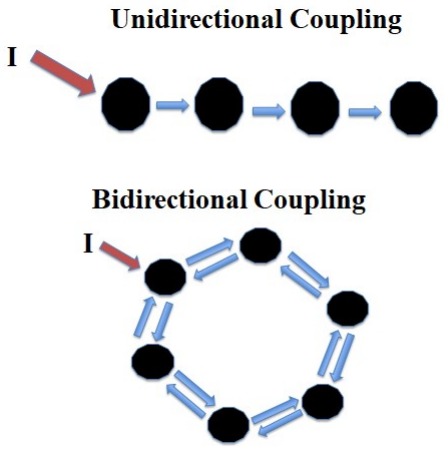

Figure 2.2: (Above) Illustration of unidirectional coupling in 4 neurons arranged in chain arrangement (Fixed boundary conditions). (Below) Illustration of bidirectional coupling in 6 neurons arranged in a ring arrangement (Periodic boundary conditions).

2.3.1 Two Parameter plots

For carrying out the parameter analysis on the Hodgkin Huxley neuron, we divided the parameter space for our model into regions of qualitatively different dynamic behaviours. In our case, we have three parameters. To visualize these regions and to note down properties associated with these regions better, we constraint one of the parameters and just look at a 2-D plot with both axes of the plot representing the two non constrained parameters. We refer to this as a two parameter plot. These plots can be used to identify regions of qualitatively different behaviours in the parameter space. We could also incorporate information on how the third parameter changes the region and its properties by changing the value of the constrained third parameter and then again looking at the behaviour of the model at different values of the other two parameters. By identifying the new region, we discover how changing the third parameter has changed the region. This process of identifying regions of qualitatively different behaviour through two parameter plots requires us to generate plots of the output value for parameter values covering the part of the parameter plane in question. This means we need to generate thousands of plots to cover the region of the parameter plane. We need to generate a plot for each parameter value set, and we need to do this by changing the parameter values to cover the whole plane. The entire process of how these plots are generated is given down below. We demonstrate the process of generating two parameter plots when we have three possible parameters. The steps of the process are

1. One parameter out of the three parameters is fixed. Now, we are constrained to move along a 2-D plane in the parameter space.

2. We now temporarily fix the second parameter too. Now we are constrained to move along a line parallel to the third parameter in the parameter space.

3. We run a loop in our code to keep changing the third parameter by small amounts, so that we cover the line that we were constrained to move on. We generate hundreds of plots to map the line completely so that we do not miss if there is a change in the dynamic behaviour at some point along this line.

4. We repeat this by changing the value for the second parameter. We keep moving along different lines in our 2-D plane. This way, we have mapped our two parameters and we know which region in this two parameter plane corresponds to what behaviour.

5. We do this for different values of the first (constrained) parameter and note down what happens to the region.

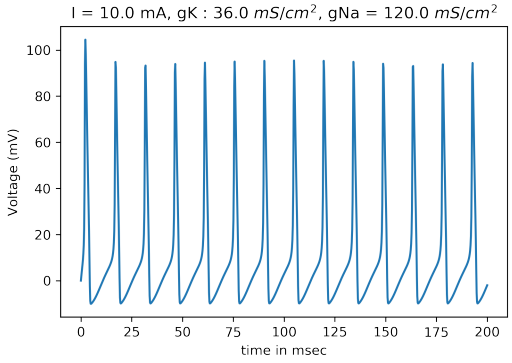

Figure 2.3: Stable self sustained action potentials (Sustained periodicity)

The above-mentioned steps essentially separate the two-parameter space into regions of different dynamical activity. The type of dynamics focused on are (i) Continuously spiking (Sustained periodicity), (ii) Steady state attractor (Fixed point dynamics), and (ii) Damped oscillations leading to steady state (damped oscillations). These three types of dynamics can be further classified into two classes:-

- Sustained action potentials - Oscillation of type (i) (Sustained periodicity). When the system shows continuous spiking behaviour in the long run, we term it as stable self

sustained action potentials. Figure 2.3 illustrates the output of the Hodgkin Huxley model for parameter values that produce stable self sustained action potentials.

- Stable dynamics/ Damped Oscillations - Oscillations of type (ii) (Fixed point dynamics) and type (iii) (Damped oscillations) as both of these display stable dynamics in the long run. These correspond to the system showing either resting potentials or graded potentials in the long run. What this means is that even if there are a few action potential peaks in the beginning as transient and then the system decays to resting potentials or graded potentials later, we classify these as stable fixed point dynamics/ Damped potentials. An illustration (Figure 2.4) showing two examples of stable behaviour is given.

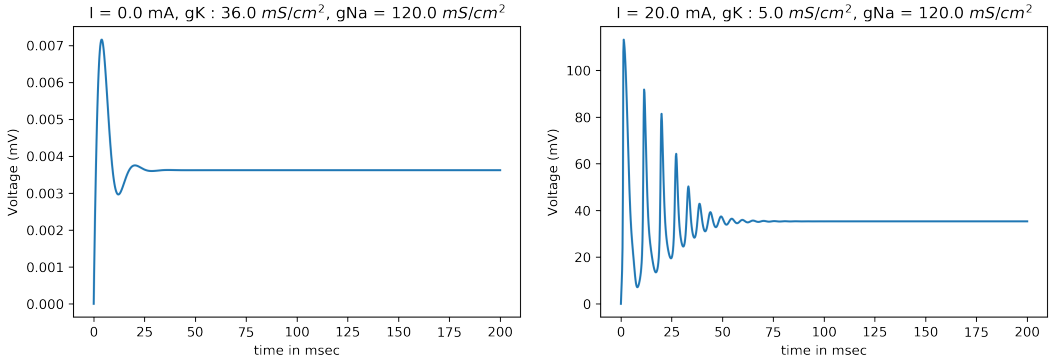

Figure 2.4: Asymptotically stable dynamics with an illustrative example of fixed point dynamics on the left and an example of damped oscillations leading to ultimately stable dynamics on the right.

2.3.2 Space Time plots

Space time plots are generated with the heatmap function in python Jupyter. Space time plots act as a qualitative way to assess synchronization in multiple coupled neurons. Following is an example of a space time plot (Figure 2.5) for ten coupled neurons. This figure is just to illustrate how a space time plot looks like. Time in msec is denoted on the X-axis. On the Y-axis, we have the neuron number, and there is a scale adjacent to the figure that indicates the intensity/ voltage. Thus, a brighter patch of light means that a neuron is firing. A darker patch means that the neuron is at low voltage (around resting potential). For neuronal networks to be synchronized, the light and dark patches must align along the Y-axis.

That would indicate that all neurons are firing at the same time.

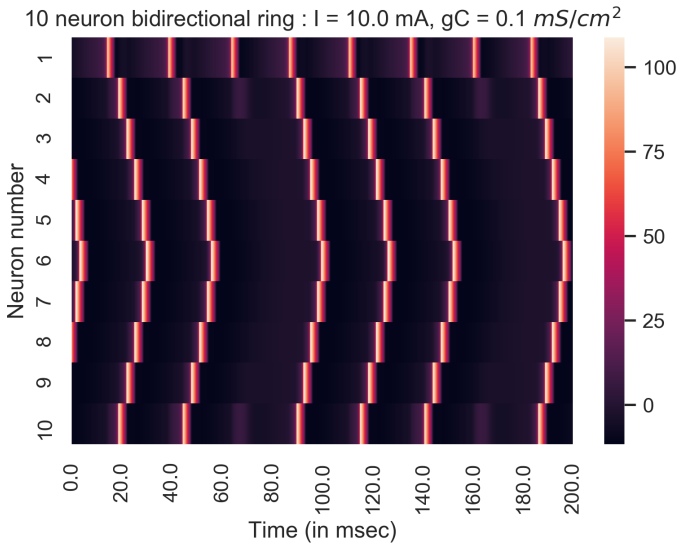

Figure 2.5: Illustration of a Space Time plot for values of I = 10.0 mA; g_C = 0.1 $\frac{mS}{cm^2}$

As can be seen in the figure, the neuronal firing is not synchronized completely as all neurons do not fire at the same time. The figure would indicate higher levels of synchronization if all the light patches were more aligned along the Y-axis.

2.3.3 Synchronization Order Parameter

A quantitative way to measure and attribute a numerical value to synchronization is through a parameter called the synchronization order parameter. The level of Synchronization depends on a lot of factors and the values of the parameters. This quantity may also be very useful in ascertaining the point at which transition from phase synchronous behaviour to complete synchronous behaviour occurs. This quantity was first used in the paper [24] and has since also been used in other works where it is used to measure synchronization in coupled cells [25]. Synchronization order parameter (R) is described as -

$$R = \frac{< M^2 > - < M >^2}{[< z_i^2 > - < z_i >^2]} \tag{2.1}$$

Note that the symbol <> denotes temporal averaging, and the symbol [ ] denotes spatial averaging. M is the spatial average over all cells for a particular time point. The Synchronization order parameter can have values between 0 and 1 (included). Higher values of R refer to higher synchronization.

Chapter 3

Dynamics of Single Neuron on Variation of Parameters

The Hodgkin Huxley model, as given in Section 2.1, is a realistic biophysical description of the ion channel activities in the neuron. The ion channels that are important in maintaining the voltage across the membrane are Sodium and Potassium ion channels as given in the first equation of the HH model:-

$$C_m \frac{dV_m}{dt} = I - g_l(V_m - V_l) - \bar{g}_{Na} m^3 h (V_m - V_{Na}) - \bar{g}_K n^4 (V_m - V_K) \tag{3.1}$$

where I is the input current, $\bar{g}_{Na}$ is the maximal conductance of the Sodium channel, $\bar{g}_K$ is the maximal conductance of the Potassium channel, g_l is the conductance of the leak channels, C_m is the value of the capacitance and V_l, V_{Na}, V_K are the reversal potentials for leak ions, Sodium and Potassium ions respectively. V_m is the value of the output Voltage across the capacitor.

To study the dependence of the neuronal dynamics on parameters, we chose three parameters, which are - (i) The maximal conductance of the Sodium channel ($\bar{g}_{Na}$), (ii) The maximal conductance of the Potassium channel ($\bar{g}_K$), and (iii) The input current (I). The other parameters are kept constant. We vary the three parameters ($\bar{g}_{Na}$, $\bar{g}_K$ and I) and record the temporal dynamics of the output Voltage variable (V_m) in the HH model for a long time to assess its stability. The aim is to divide the parameter space into regions of qualitatively different dynamical behaviours.

As mentioned in subsection 2.3.1, we look for two types of long-term behaviour in the time series of the membrane potential (V_m). So the initial transient behaviour is not considered

while assessing the qualitative behaviour of the system. Here we present the results for the long-term dynamical behaviour of the neuron under different parametric conditions. Since we are considering the long-term behaviour of the system, we take the input current at a constant value for the whole time period. Based on this, we classify the activity of a single neuron into two types - (A) stable (or, fixed point) with or without damped oscillations, and (B) sustained oscillations (periodic). For every combination of parameters, the long-term dynamics in Voltage was noted and grouped into any one of the two classes. Illustrations for visually depicting these have been given in Figures 2.2 and 2.3 in subsection 2.3.1.

Along with the type of dynamics, the frequency and amplitude of the action potentials are also important properties to be studied. First, we ascertain the dependence of the frequency of firing in the HH neuron on the constant input current parameter (I) given to the neuron (see Eqn. 3.1). Figure 3.1 is a plot where the Y-axis depicts the number of action potentials in a 125 msec interval and the X-axis depicts the corresponding constant input current value. Here, the $\bar{g}_{Na}$ and $\bar{g}_K$ values are chosen such that they lead to stable sustained action potentials/ oscillations for the tested input current range (X-axis).

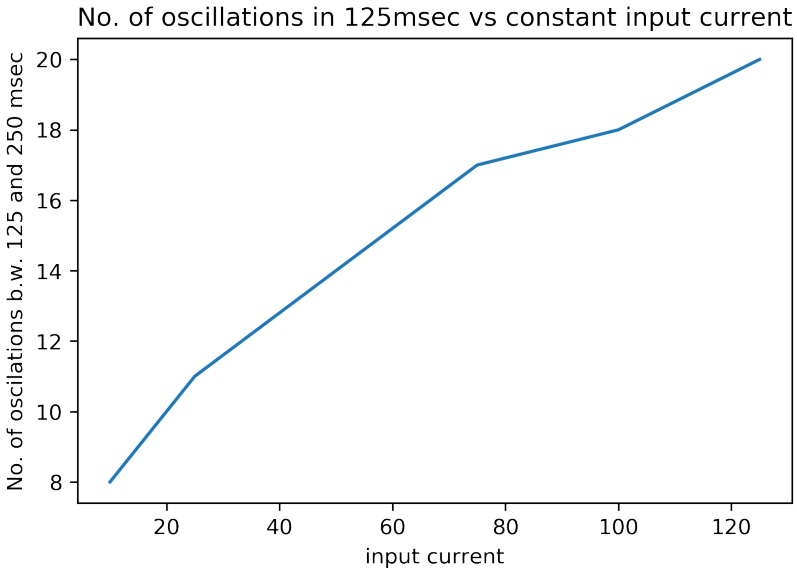

Figure 3.1: Dependence of frequency of action potential generation on input current value for value of $\bar{g}_K = 36.0\ \frac{mS}{cm^2}$ and $\bar{g}_{Na} = 120.0\ \frac{mS}{cm^2}$

The figure clearly shows that the spiking frequency of action potential increases with increasing input current.

3.1 The Potassium conductance ($\bar{g}_K$) - Input current (I) parameter plot

To understand the 3-dimensional parameter space, the first step we took is to plot the spike dynamics by changing two parameters ($\bar{g}_K$ and I) with the third parameter ($\bar{g}_{Na}$) kept at a constant value. This is then repeated with a different value of the third parameter. That can give some idea of how the parameters affect the type of the spike dynamics.

3.1.1 Dividing the $\bar{g}_K$-I plane into regions of qualitatively different dynamics

In the previous section, we discussed what we meant by qualitatively different dynamical behaviours for a single neuron. We divide the $\bar{g}_K$-I (Potassium conductance - Input current) plane into regions of qualitatively different dynamical behaviours following the method described in subsection 2.3.1. Figure 3.2 denotes this region for the fixed $\bar{g}_{Na}$ value (Sodium conductance value) of 120.0 $\frac{mS}{cm^2}$. We find that there exists a bounded region in the $\bar{g}_K$-I plane, inside which the single neuron generates sustained oscillations/ stable self sustained action potentials. Outside this region, the behaviour is always fixed point dynamics. Thus, outside this region either stable fixed points dynamics is observed or damped potentials leading up to an asymptotic stable state is observed and we refer to this collectively as the damped oscillation behaviour. For a fixed $\bar{g}_{Na}$ value, the bounded curve consists of two sets of transitions shown by orange and blue points with increasing input current (I). The red line parallel to the X-axis denotes 0.0 value of input current. The first set of transitions, at low I, is denoted in the figure with an orange set of points. This set of transitions is from damped potentials to stable self sustained action potentials. The second set of transitions from stable self sustained action potentials back to damped potentials is denoted by the blue set of points.

This indicates that stable self sustained action potentials is only possible inside this bounded region of parameter sets, for a fixed $\bar{g}_{Na}$ value. The shape of the bounded region also shows that for medium values of potassium conductance, the neuron shows sustained spikes for a larger range of input currents compared to both lower and higher values of potassium conductances.

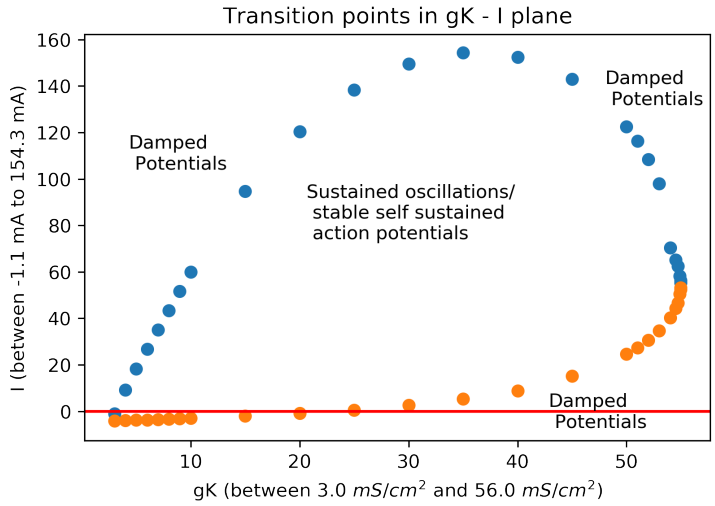

Figure 3.2: $\bar{g}_K$-I parameter plane for $\bar{g}_{Na} = 120.0\ \frac{mS}{cm^2}$

3.1.2 Effect of Sodium conductance ($\bar{g}_{Na}$) on the $\bar{g}_K$-I parameter plot

To determine the effect of varying the maximal sodium conductance on the bounded region of stable self sustained action potentials, the same plot was calculated on another value of $\bar{g}_{Na}$. Figure 3.3 shows the results.

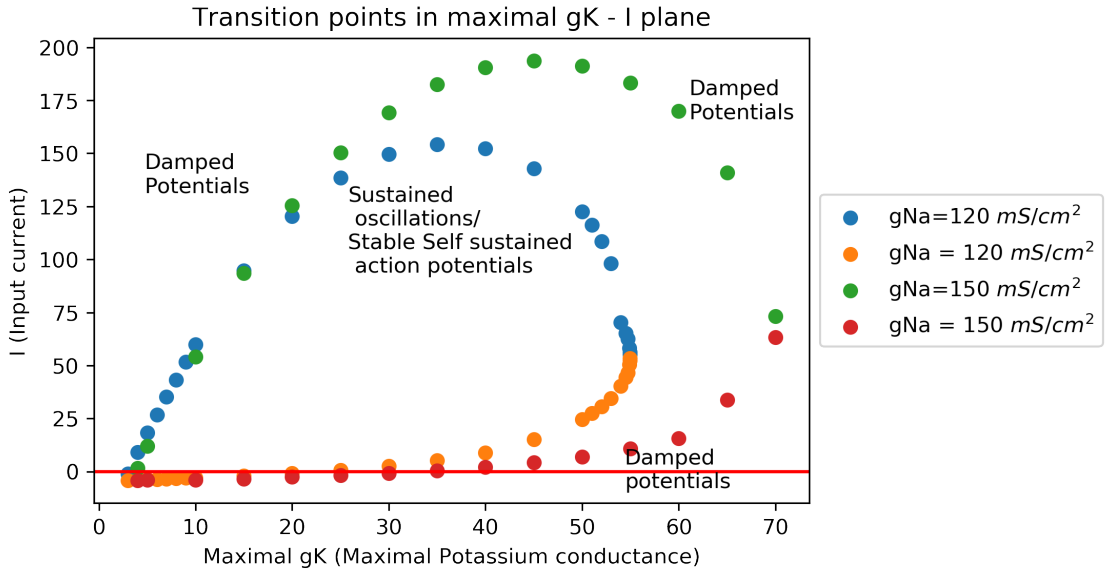

Figure 3.3: $\bar{g}_K$-I parameter plane for $\bar{g}_{Na} = 120.0$ and $\bar{g}_{Na} = 150.0\ \text{mS}\frac{}{cm^2}$

As can be seen from the figure, even though the shape of the bounded region is very similar in both cases, the area of the bounded region increases with higher maximum possible value of sodium conductance ($\bar{g}_{Na}$). The leftmost point where both these curves start, al-

most overlap in both cases. However, the total area enclosing the region of stable self sustained action potentials is larger for higher maximal sodium conductance values.

If one were to intuitively guess of what would happen to the bounded region on increasing maximal sodium conductance, one would have guessed that the area would increase. This is because Sodium ions are responsible for eliciting action potential generation. Thus, higher Sodium conductance would mean that it would be easier for the neuron to generate action potentials and thus, stable self sustained action potentials. Thus action potentials would be generated for higher values of maximal potassium conductance and input current values giving a larger bounded area for sustained action potentials in the $\bar{g}_K$-I plane. Also, it is important to note that nonlinear systems are extremely complex, and it may be difficult to directly intuitively predict behaviour of a system. Thus, computational modelling and simulations are essential to know the behaviour of nonlinear systems.

3.1.3 Properties of the dynamical transitions in the $\bar{g}_K$-I parameter plane

In Figure 3.3, for $\bar{g}_{Na} = 120.0\ \frac{mS}{cm^2}$, the boundaries are made up of two curves, which denote two different dynamical transitions. For a particular $\bar{g}_{Na}$ value, the first set of transition points (represented in orange) denotes the transition from damped potentials (outside) to stable self sustained action potentials (inside). The second set of points (denoted by blue) are transitions from stable self sustained action potentials (inside) to damped potentials again outside the bounded region. We look at both these sets of transitions and elaborate their properties. To check the properties of each transition point, we adopted the following procedure.

- A value for maximal potassium conductance should be fixed, and looking at the graph; one should first ascertain the corresponding value for the input current for which the transition occurs.
- At the transition point coordinates decided by the previous step, we need to figure out whether each of those transitions is marked by an abrupt change in the qualitative behaviour of the system (damped and stable self sustained action potentials are the two types of behaviours) or a more continuous and gradual change in the qualitative

behaviour of the system when changing the input current parameter. We consider the amplitude of oscillations in the long run as an indicator of whether the transition occurs abruptly by a sudden change in amplitude of oscillations or the transition is more gradual with the amplitude of oscillations gradually dying out to a resting state potential with changing input current parameter.

- We repeat this for all the points and try to ascertain a pattern.

Repeating the steps mentioned above on each point in both the upper and lower transition point sets, we find the following results for each sets of points.

1. The first set of points (denoted in orange) all follow an abrupt transition for a small change in input current (I) value across the border. This is because the amplitude of oscillations in the long run suddenly and abruptly changes in these sets of points as shown in Figure 3.4. These figures denote how the amplitude suddenly and abruptly rises at the transition point upon a small increase in the input current.

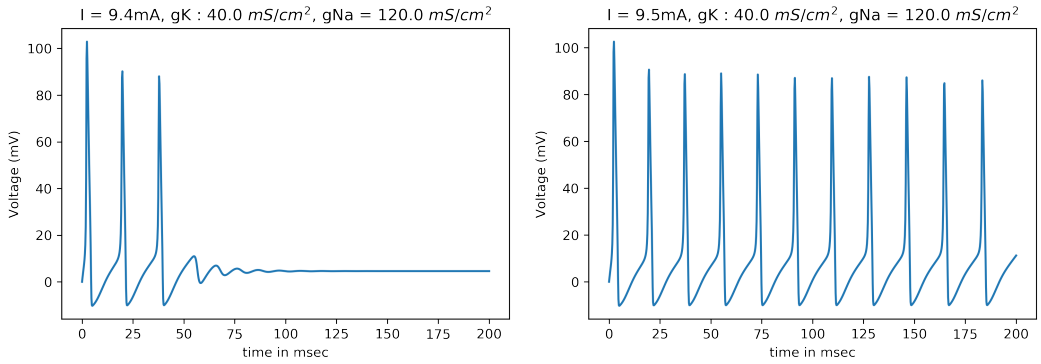

Figure 3.4: Abrupt change in the dynamic behaviour of the system for the first transition from damped potentials to sustained oscillations with a small change of 0.1 mA (from I = 9.4 mA in the first plot to I = 9.5 mA in the second plot) in the Input current parameter

2. The second set of points in blue follow a more interesting set of properties. Unlike the first set of points (orange), here all the transitions are not abrupt. Instead, we find that transitions are abrupt for lower values of maximal potassium conductance ($\bar{g}_K$) as illustrated in Figure 3.5, and for higher values of maximal potassium conductance ($\bar{g}_K$), we get continuous and gradual transitions as illustrated in Figure 3.6.

   The properties could be assessed in more detail by plotting the amplitudes just before the transition and just after the transition by varying input current about the transition

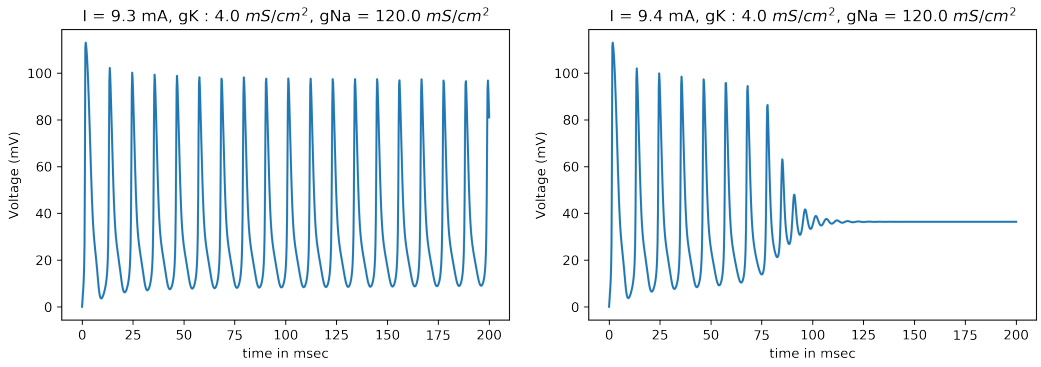

Figure 3.5: Abrupt change in the dynamic behaviour of the system for the second transition from sustained oscillations to damped potentials with a small change of 0.1 mA (from I = 9.3 mA in the first plot to I = 9.4 mA in the second plot) in the Input current parameter. This abrupt change in dynamics occurs for lower $\bar{g}_K$ values.

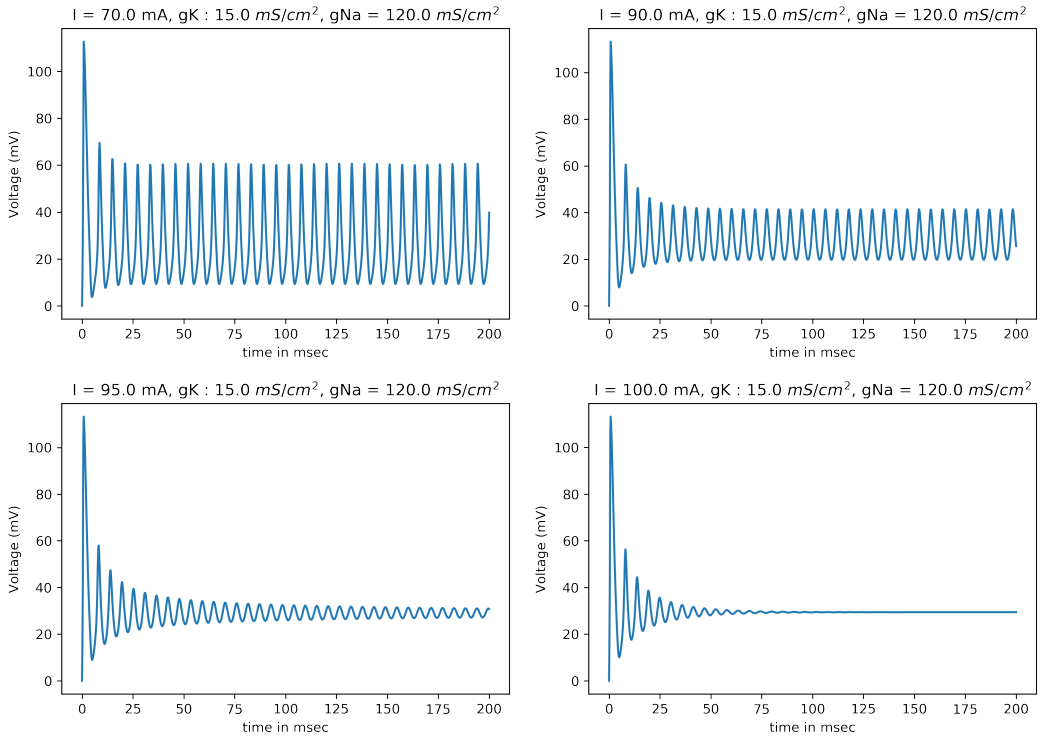

Figure 3.6: Gradual change in the dynamic behaviour of the system with Input current parameter for the second transition from sustained oscillations to damped potentials. This continuous and gradual change in dynamics occurs for higher $\bar{g}_K$ values

point (Figure 3.7). For the second set of points (in blue), which indicate transition from stable self sustained action potentials inside the bounded region to damped oscillations outside, we notice that the amplitude of the sustained spiking just before the

transition (inside the bounded region) decreases with increasing $\bar{g}_K$ value. Outside the bounded region, the damped potentials reach a resting state potential behaviour asymptotically. Figure 3.7 shows the long-term value of the maximum and the minimum of the action potentials reached before the transition, i.e. inside the boundary, and the value of resting potential attained for damped potentials after the transition (outside the region) for different values of $\bar{g}_K$ at the blue (upper) transition points of Figure 3.2.

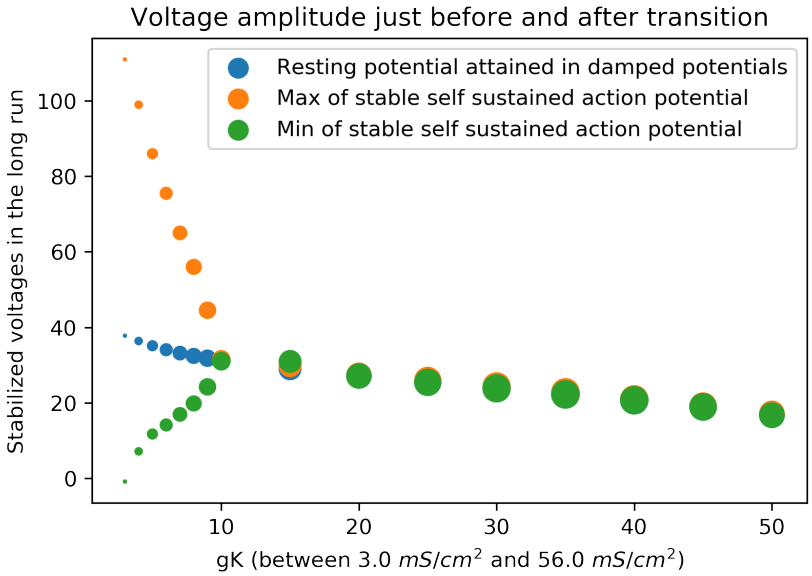

Figure 3.7: Probing the amplitude of oscillations at the point of transition for $\bar{g}_{Na} = 120.0$ $\frac{mS}{cm^2}$

Note that Figure 3.7 has Voltage values on the Y-axis and maximal potassium conductance values on the X-axis. Whenever we fix the maximal potassium conductance value, we also fix the value of Input current at which transition happens. Thus, the X-axis denotes not just $\bar{g}_K$, but it also fixes the current value at which the transition from sustained oscillations to damped oscillations occurs. The input current value is ascertained from Figure 3.3 (blue points), and this information for the input current is incorporated in the plot (Figure 3.7) by scaling the size of the points according to the input current values with larger dots indicating a higher value of input current at which transition occurs. This illustration is for $\bar{g}_{Na} = 120.0$ $\frac{mS}{cm^2}$. The orange points in Figure 3.7 indicate the maximum value of stable self sustained action potentials just before the transition while the system is inside the bounded region. Similarly,

the green points are for the minimum voltage value for the stable self sustained action potentials. The blue set of points indicates the value for resting potential that the system attains just after transition upon going into the region of damped potentials. We notice that all three points coincide for values of $\bar{g}_K \geq 10\ \frac{ms}{cm^2}$. Thus this result states that for the second set of transitions (blue points), there is a continuous change in amplitude with input current for $\bar{g}_K >= 10\ \frac{ms}{cm^2}$. Also, there is an abrupt change in amplitude for $\bar{g}_K < 10\ \frac{ms}{cm^2}$.

3.2 The Potassium conductance - Sodium conductance parameter plane

Now, we look at the $\bar{g}_K - \bar{g}_{Na}$ parameter plane for constant input current (I) values fixed. As in the previous section, we do this study for different fixed values of the third variable, the input current (I), and then look at their effect on the regions of qualitatively different dynamical behaviours.

3.2.1 The $\bar{g}_K - \bar{g}_{Na}$ plane and effect of input current (I) values

The steps taken for identifying the curves of transition are the same as before. The effect of input current on the bounded region is probed by repeating the following steps for each value of the input current (I).

- Fix the input current value.
- Fix $\bar{g}_K$ and vary $\bar{g}_{Na}$ to identify points of transition along the $\bar{g}_{Na}$ axis.
- Repeat this for different $\bar{g}_K$ values, thus covering the $\bar{g}_K - \bar{g}_{Na}$ plane.
- Change the input current value and repeat from step 1.

The results obtained are shown in Figure 3.8.
The figure suggests that unlike the $\bar{g}_K - I$ plane, the $\bar{g}_K - \bar{g}_{Na}$ plane is not bounded on all sides. It is bounded on three sides only. Here also, we get a series of two transitions when we move along the Y-axis ($\bar{g}_{Na}$) for every $\bar{g}_{Na}$ value. We do not see a very major effect of changing input current on the region except that there are slight shifts in the curves forming

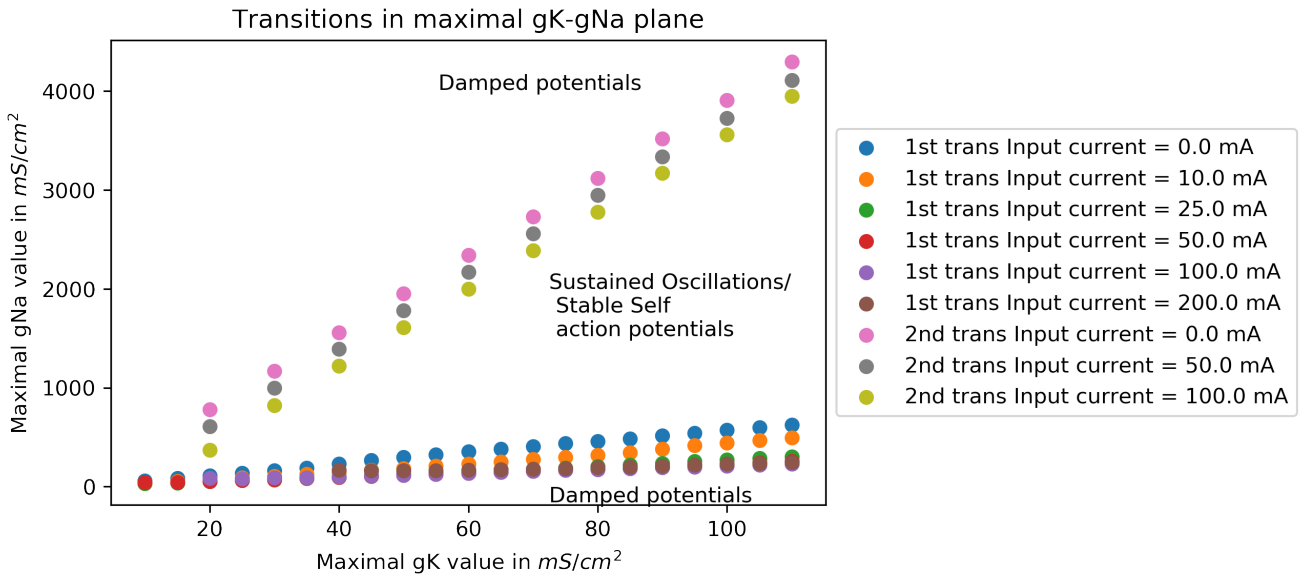

Figure 3.8: Dynamical regions in the $\bar{g}_K - \bar{g}_{Na}$ plane for different I

the boundaries of the region of stable self sustained action potentials. This major difference from the $\bar{g}_K$-I curve is that there is no limit to the $\bar{g}_K$ value (in the range studied) for obtaining stable self sustained action potentials for a given $\bar{g}_{Na}$ value. Another difference in the $\bar{g}_K - I$ and the $\bar{g}_K - \bar{g}_{Na}$ parameter plots is that their boundaries are different. While the boundaries for $\bar{g}_K - I$ plane were closed curves, the boundaries for $\bar{g}_K - \bar{g}_{Na}$ plane are almost straight lines. We discuss their dynamical behaviour in the next subsection.

3.2.2 Effect of Input Current (I) on transitions in the $\bar{g}_K - \bar{g}_{Na}$ plane

A similar analysis of the changes in the maxima and minima of the amplitude of oscillations at each of the transitions could be done. However, here we show the effect of the input current on the position of the transition curves in the $\bar{g}_K - \bar{g}_{Na}$ plane. Firstly, an expanded view of Figure 3.8 is given in Figure 3.9 (A and B).

1. The expanded view of the first set of transition points can be seen in Figure 3.9 (A). We probe the effect of changing input current on the curve that joins these transition points. We can approximate these curves as straight lines even though we see higher bending in curves for higher input current values. This bending effect can be clearly seen to start with the red points (I = 50.0 mA), and it progressively increases with increasing input current values with a significant initial bend seen in high input current values corresponding to 200.0 mA (brown points). These bends are however, present

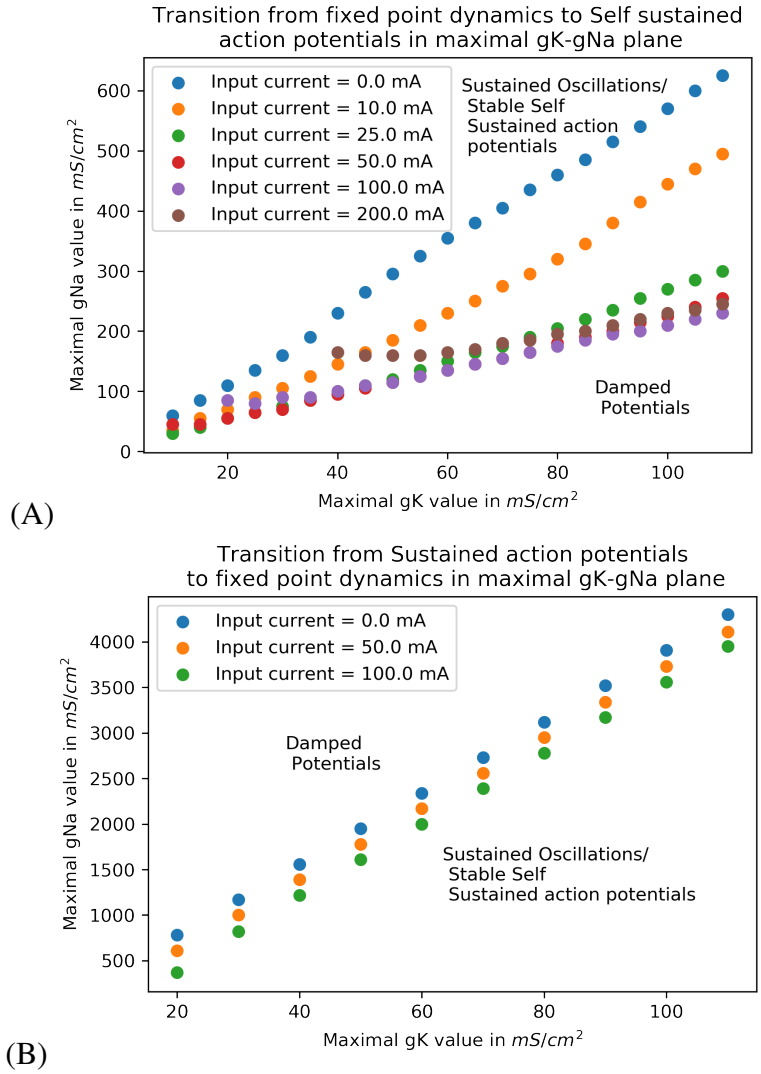

Figure 3.9: Expanded view of the transition curves. (A) Lower transition points; (B) Higher transition points

at the beginning of the curves, and they approximate to the shape of a straight line, if we consider points of higher $\bar{g}_K$ values. Approximating these curves as straight lines, it can be seen that the slope of the straight line decreases with increasing input current. The slope does not change linearly with increasing input current. It instead converges to a value. The decrease in the slope was really high on a jump from input current magnitude from 0.0 (blue) to 10.0 (yellow). The decrease in slope is still noticeable even for the jump from 10.0 to 25.0 (green). However, the slopes for the input current magnitude of 25.0, 50.0, 100.0, and 200.0 are almost the same, and a significant change in slope is not seen even with a 100.0 mA jump. Thus the slope converges to a constant value.

2. The second set of transition points shown in Figure 3.9 (B) are from stable self sustained action potentials to damped potentials. As can be seen from the plot, these transition points lie very well along straight lines. No bend is visible in this range of points. Interestingly, when we try to see the effect of changing input current on the straight lines, we see that unlike in the previous case, their slope does not change. Instead, the value of the constant of the line changes, and the lines just shifts down with increasing input current. Additionally, the shift seems to vary linearly with increasing input current.

3.3 Summary

We mapped the three dimensional ($\bar{g}_K$, $\bar{g}_{Na}$, I) parameter space of the single Hodgkin Huxley neuron using two parameter plots. We probe the effect of the third parameter on regions of qualitatively different dynamical behaviours in these two parameter planes. Moreover, we identify properties for transition points using change in amplitude of oscillations as a parameter. Salient features of the parameter space with respect to evolution of different dynamical behaviours are mapped at a fine scale and combination of three parameters obtained for describing changes in dynamics. These changes are elaborated from the manner at which dynamics changes from stable to sustained oscillations by considering amplitude change in voltage (V) as a read-out parameter. The implications are described in the final Discussion section from both bifurcation and type of phase transition point of view. Thus, in this section, we have successfully mapped the parameter space of the single Hodgkin Huxley neuron and some of its properties. This prepares us to study the properties of multiple neurons.

Chapter 4

Dynamics of Two Coupled Neurons on Variation of Parameters

Neurons communicate with each other through chemical and electrical synapses. An important feature that distinguishes electrical synapses from chemical synapses is that the former can be both unidirectional and bidirectional, while chemical synapses are mostly unidirectional synapses. The coupling through an electrical synapse is via gap junctions, which are channels (made of proteins) between cells. In this section, we have studied the dynamical properties of two neurons coupled with the help of an electrical synapse. We are particularly interested in understanding "synchronization" (see section 1.4 of Chapter 1) of electrical activity of the two neurons and its dependence on various cellular parameters. The aim is to study how the strength of electrical coupling (g_C) and their types (unidirectional or bidirectional) alter the firing patterns of the individual neurons in a two-neuron system. Here, and in the next chapter, we study the effect of these parameters on synchronization in the system of coupled neurons. When a neuron is connected/coupled to another neuron, it receives additional electrical current ($I_{electrical}$) due to the coupling. In general, the membrane voltage variation in a Hodgkin Huxley neuron, with input current (I), connected with an electrical synapse, can then be modelled by:

$$C_m \frac{dV_m}{dt} = I - I_{ionic} - I_{electrical} \tag{4.1}$$

The other equations (Eqn number 2 to 10 in section 2.1) remain the same. $I_{electrical}$ is modelled based on the type of coupling, i.e., whether coupling is unidirectional or bidirectional. In chapters 4 and 5, we present dynamical behaviour exhibited by the system of neurons

for different types and strengths of electrical synapses, with varying boundary conditions (ring-like or chain-like connectivity) and network size (number of neurons), and show how these parameters affect synchronization of neuronal activity based on both qualitative and quantitative analysis. In this chapter, we start with the simplest network of two neurons that can be coupled unidirectionally or bidirectionally through gap junctions. Below, we first discuss the models for unidirectional and bidirectional couplings, and then show an overall representation of the effect of input current on the action potentials of the two neurons. Results on frequency synchronization, and phase synchronization in two electrically coupled neurons are discussed in detail.

Consider two neurons, with the voltage across neuronal membrane of first neuron as V_1 and that across the second neuron as V_2. These two neurons can have unidirectional coupling where only the voltage of one neuron (say, the first neuron (V_1)), affects the second neuron. As mentioned before, now an extra term corresponding to current due to the electric synapse ($I_{electrical}$) comes into the picture. $I_{electrical}$ is defined as the product of the gap junctional conductance between the two neurons, and their voltage difference, i.e., ($g_C(V - V_{adjacent})$). Here, $V_{adjacent}$ is the voltage of the adjacent neurons that are connected through the gap junction. The parameters that can be changed for two neurons are either the coupling strength (g_C), or, the magnitude of input current in the driving neuron 1 (I), or, the type of coupling (unidirectional and bidirectional). We look at both qualitative and quantitative methods to measure each neuron's dynamics and their synchronization.

Unidirectionally coupled neurons

We have two neurons. Neuron 1 makes an electrical synapse with neuron 2 with current flowing only in one direction - neuron 1 to neuron 2. Considering the neuronal membrane voltages of first neuron as V_1 and that for the second neuron as V_2 , the revised HH equations for this coupled two-neuron system are :-

- For the first neuron -

$$C_m \frac{dV_1}{dt} = I - I_{ionic} \tag{4.2}$$

- For the second neuron -

$$C_m \frac{dV_2}{dt} = -I_{ionic} - I_{electrical} \tag{4.3}$$

Note that only the first neuron has an input current (I), while the other neuron does not have an input current. Thus the first neuron's input current is responsible for generating the action potentials, and it is referred as the **driving/driver** neuron. The second neuron gets the external current only through the electrical synapse ($I_{electrical}$), and is thus called the **driven** neuron (as it is being driven by the first neuron). In case of bidirectional coupling (discussed in the subsequent point), however, the second neuron also has an effect on the first neuron.

Bidirectionally coupled neurons

In bidirectional coupling of two neurons, even though only Neuron 1 gets the input current (I), yet unlike the previous case, here both the neurons have electrical coupling ($I_{electrical}$) between each other. Thus the neuron 1, which has an input current, is responsible for generating the action potentials first, and can still be called the **driving neuron**. However, even though neuron 2 is the **driven neuron**, yet due to the bidirectional coupling its electrical activity in turn affects neuron 1.
For bidirectionally coupled neurons, the driving neuron 1 is also affected by the electrical activity of the driven neuron 2. The HH equations for the two neurons are -

- For the first neuron -

$$C_m \frac{dV_1}{dt} = I - I_{ionic} - I_{electrical} \tag{4.4}$$

- For the second neuron -

$$C_m \frac{dV_2}{dt} = -I_{ionic} - I_{electrical} \tag{4.5}$$

The two types of coupling can have differential effects in the emergent properties of the firing patterns of the neurons. Figure 4.1 gives an idea of the nature of long-term action potential generation in both the neurons connected via bidirectional coupling strength, $g_C = 0.7\ \frac{mS}{cm^2}$ and for different values of input current. The figure is given only to illustrate the

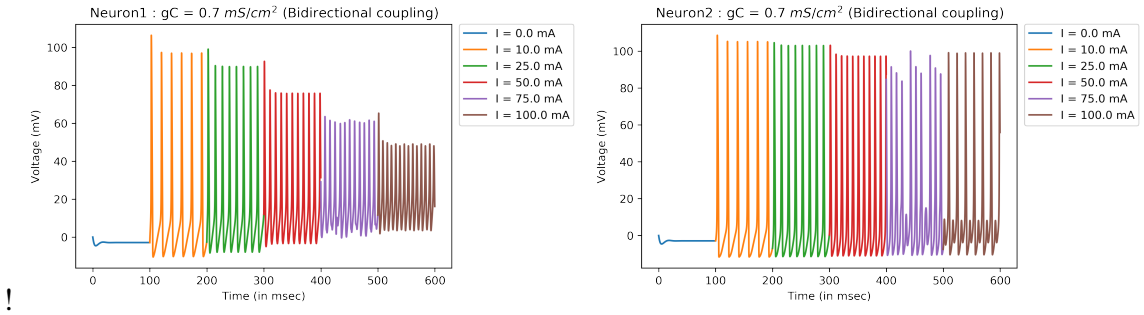

!

Figure 4.1: (Left) Time series depicting the firing pattern of the first neuron, (Right) Time series depicting the firing pattern of the second neuron for different input currents in the first neuron. The coupling type is bidirectional with coupling strength, $g_C = 0.7\ \frac{mS}{cm^2}$

pattern of firing in both the neurons. The driving neuron 1 shows higher frequency with reduced amplitude of spikes with increasing input current (I). The second neuron, which is driven by neuron 1, exhibits higher amplitude spikes but the same frequency from I = 0 to 50 mA, beyond which the two neurons show different firing patterns at this g_C. This shows that both input current and the gap junctional coupling strength have significant roles to play in the collective electrical activity of the two-neuron system. Below we present the results for the dynamics and synchronization in the two-neuron system for changing the coupling strength (g_C) and the input current (I) for the two types of coupling - unidirectional and bidirectional.

4.1 Frequency synchronization in two neurons

Frequency matching is an indicator of synchronization, so we study frequency synchronization for the two types of couplings.

4.1.1 Unidirectionally coupled neurons

HH equations for this coupled two-neuron system are :-

- For the first neuron -

  $C_m \frac{dV_1}{dt} = I - I_{ionic}$

  $C_m \frac{dV_1}{dt} = I - g_l(V_1 - V_l) - \bar{g}_{Na} m^3 h (V_1 - V_{Na}) - \bar{g}_K n^4 (V_1 - V_K)$

- For the second neuron -

$$C_m \frac{dV_2}{dt} = -I_{ionic} - I_{electrical}$$
$$C_m \frac{dV_2}{dt} = -g_l(V_2 - V_l) - \bar{g}_{Na} m^3 h (V_2 - V_{Na}) - \bar{g}_K n^4 (V_2 - V_K) - g_C(V_2 - V_1)$$

We count the number of action potentials generated in both of the unidirectionally coupled Hodgkin Huxley neurons in a 125 msec time interval. These observations are recorded for different g_C and input current (I) values. The result is shown in Figure 4.2.

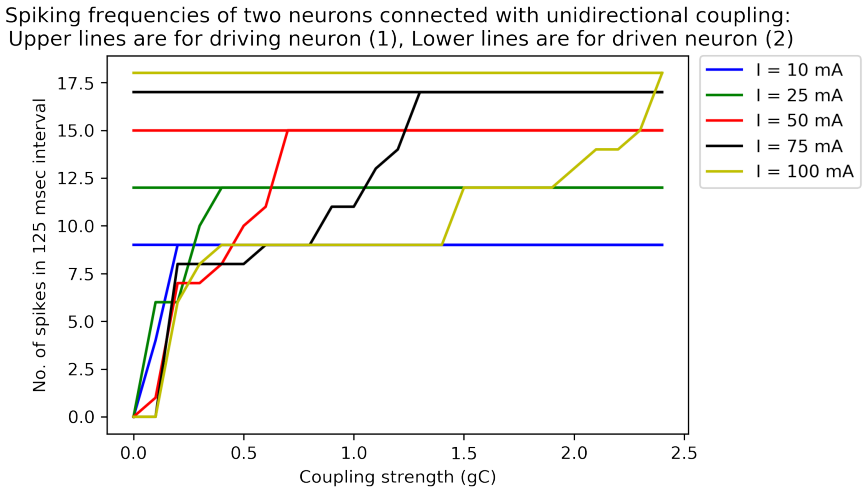

Figure 4.2: Effect of g_C on the long term action potential frequencies in the driving neuron 1 (top lines) and driven neuron 2 (lower lines) for different input currents for unidirectional coupling. Frequency synchronization is observed when both lines meet.

The X-axis in Figure 4.2 denotes the conductance values (g_C) for the electrical synapse. We have two lines for each current (I) value shown by different colours. The lines plot the number of action potentials generated in the neurons in a 125 msec time interval. For each colour (i.e., for a particular value of I), the lines coming from higher up are for the driving Neuron 1, and the ones from down below are for the second (driven) Neuron 2.
The lower lines all originate from zero, i.e., no coupling, because the neuron 2 remains silent (at resting state) without any external input current. As shown in Chapter 3, higher input currents result in higher frequency of firing of single neurons. This is clearly seen for the neuron 1's spike frequencies for different input currents (top lines). Higher the input current in neuron 1, higher is its frequency of sustained action potentials.
The following are the major observations.

1. **Effect of the coupling strength (g_C) :**

   The plots in Figure 4.2 show that, for all I values at lower gap junctional conductance

(g_C), the the two neurons continue to spike at different frequencies. Their frequencies start matching, with increasing g_C value, which indicates frequency synchronization. The frequency of the driving neuron does not change with g_C values, since it is unaffected by the unidirectional coupling, and is totally decided by the input current. The frequency of the driven neuron, on the other hand, keeps increasing with increasing g_C until it equals the frequency of the driving neuron. Thus, increasing coupling (g_C) facilitates synchronization of two unidirectionally coupled neurons, and for every driving frequency (determined by input current), there is a specific coupling strength for obtaining frequency synchronization..

2. **Effect of the Input current (I) -** For the driving neuron 1, higher frequency sustained action potentials are observed for increased input current. Neuron 2 is at rest at g_C = 0 (no coupling). This makes the difference in frequency of the two neurons higher as I increases. It is seen from Figure 4.2 that larger difference in frequency, due to higher input current in the driving neuron requires higher value of coupling strength, g_C, at which the two neurons attain the same frequency (frequency synchronization). Larger coupling is required between the two neurons to attain frequency synchronization in unidirectional coupling.

   Thus, in a unidirectionally coupled two-neuron system, even low coupling can elicit frequency synchronization if the driving neuron has low input current. Higher the input current, harder it becomes to synchronize the frequencies in this case.

4.1.2 Bidirectionally coupled neurons

The HH equations for each of the bidirectionally coupled neurons is :-

- For the first neuron -

  $C_m \frac{dV_1}{dt} = I - I_{ionic} - I_{electrical}$

  $C_m \frac{dV_1}{dt} = I - g_l(V_1 - V_l) - \bar{g}_{Na} m^3 h(V_1 - V_{Na}) - \bar{g}_K n^4 (V_1 - E_K) - g_C(V_1 - V_2)$

- For the second neuron -

  $C_m \frac{dV_2}{dt} = -I_{ionic} - I_{electrical}$

  $C_m \frac{dV_2}{dt} = -g_l(V_2 - V_l) - \bar{g}_{Na} m^3 h(V_2 - V_{Na}) - \bar{g}_K n^4 (V_2 - E_K) - g_C(V_2 - V_1)$

The results for the effect of g_C and input current value on synchronization are shown in

Figure 4.3. The lower lines for neuron 2 still originate from zero at $g_C = 0.0$, as there this neuron is at rest without any input current due to the absence of the electrical synapse. The following are the major observations.

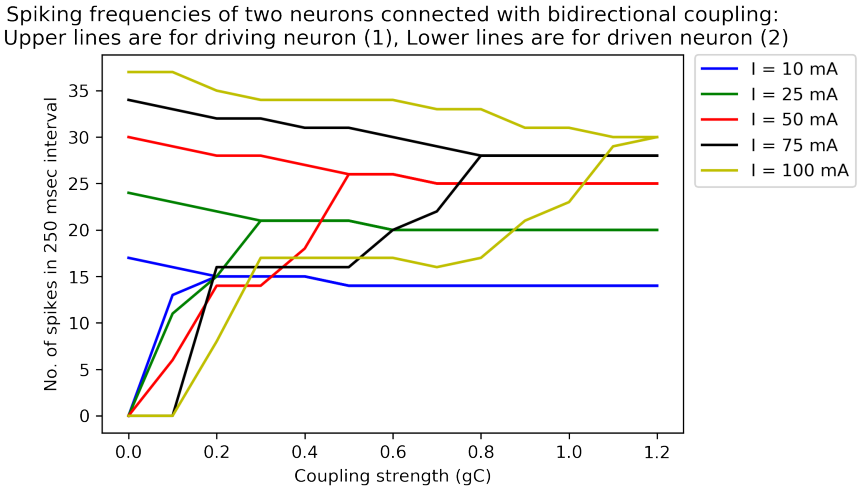

Figure 4.3: Effect of g_C on the long term action potential frequencies in the driving neuron 1 (top lines) and driven neuron 2 (lower lines) for different input currents for bidirectional coupling. Frequency synchronization is observed when both lines meet.

1. **Effect of the coupling strength (g_C) :** Like uni-directional coupling, here also, the two neurons continue to spike at different frequencies at lower g_C for all input currents, and their frequencies synchronize with increasing g_C value. However, due to the effect of the neuron 2 on the driving neuron 1 for bidirectional coupling, the frequency of the driving neuron 1 keeps decreasing with increasing g_C value. Interestingly, compared to uni-directional coupling, frequency synchronization occurs at lower coupling strengths when bidirectional coupling is present, for the same input current. Thus, bidirectional coupling facilitates frequency synchronization in two neurons at lower g_C values. Note that the number of oscillations denoted on the Y-axis for the case of unidirectional coupling is for a 125 msec time interval, while for the bidirectional case it is for a 250 msec interval. This has been done to clearly show the effect of decrease in the frequency of the action potentials in neuron 1 with increasing g_C values.

2. **Effect of the input current (I) in neuron 1 -** All results obtained for unidirectional coupling are observed here with one noticeable difference. In the former case (uni-

directional), both neurons locked frequency at the frequency of the driving neuron 1 for all values of I. Here, for bidirectional coupling, both neurons, even after getting synchronized, continue to decrease their frequencies with increasing g_C values for lower input currents, after which the frequencies do not change with increasing coupling. Thus, bidirectional coupling not only allows frequency synchronization at lower gap-junctional conductances of the electrical synapse for all input currents, it also adapts both the driving and driven neurons to exhibit synchronized electrical activity at a lower frequency value than decided by the input current. This property of the two-neuron system is an emergent adaptive feature of this small electrical network.

4.2 Phase Synchronization and Complete Synchronization in two neurons

This section highlights the occurrence of two major types of dynamical behaviours in the 2 neuron system - (i) Phase synchronization, and (ii) Complete synchronization. In the context of the two neuron system, phase synchronization is observed when both neurons spike continuously and the time period of spiking is the same for both neurons but there is a lag associated between the firing activity of the two. Complete synchronization in two neurons occurs when both neurons achieve an identical and overlapping pattern of spiking and there is no lag present. We use a space time plot (refer to section 2.3.2) to describe the long-term electrical activity of the two neurons in both space and time. They are shown as heat maps of voltages of the action potentials in two neurons. These maps are helpful in qualitatively indicating the two types of synchronization (Phase and Complete Synchronization) in coupled neuron systems. If the heat maps have the activity of the neurons properly aligned (i.e - aligned dark and bright patches) along the y-axis, this is an indicator of complete synchronization. The presence of a phase difference between the two neurons shows in the heat maps as a lag in the activity of the driven neuron 2 as compared to the driving neuron 1 (i.e - bright patches for the second neuron occur after a delay from the occurrence of bright patches in the first neuron) and this indicates phase synchronization.
The results for space time plots for different g_C values and different input current values in the driving neuron 1 are given below for unidirectional and bidirectional couplings for

three different input currents (I=10.0 mA, 25.0 mA and 50.0 mA). For each input current, a large range of g_C values were checked from 0.0 to 1.0 $\frac{mS}{cm^2}$ at a gap of 0.1 $\frac{mS}{cm^2}$ between each successive observation.

4.2.1 Input current in driving neuron 1 : 10.0 mA

Unidirectional coupling

The space-time plots for $I = 10.0$ mA in the driving neuron 1 for unidirectional coupling are given in Figure 4.4 for four increasing g_C values. The X-axis is time and Y-axis shows the amplitude of action potentials in neuron 1 and neuron 2.

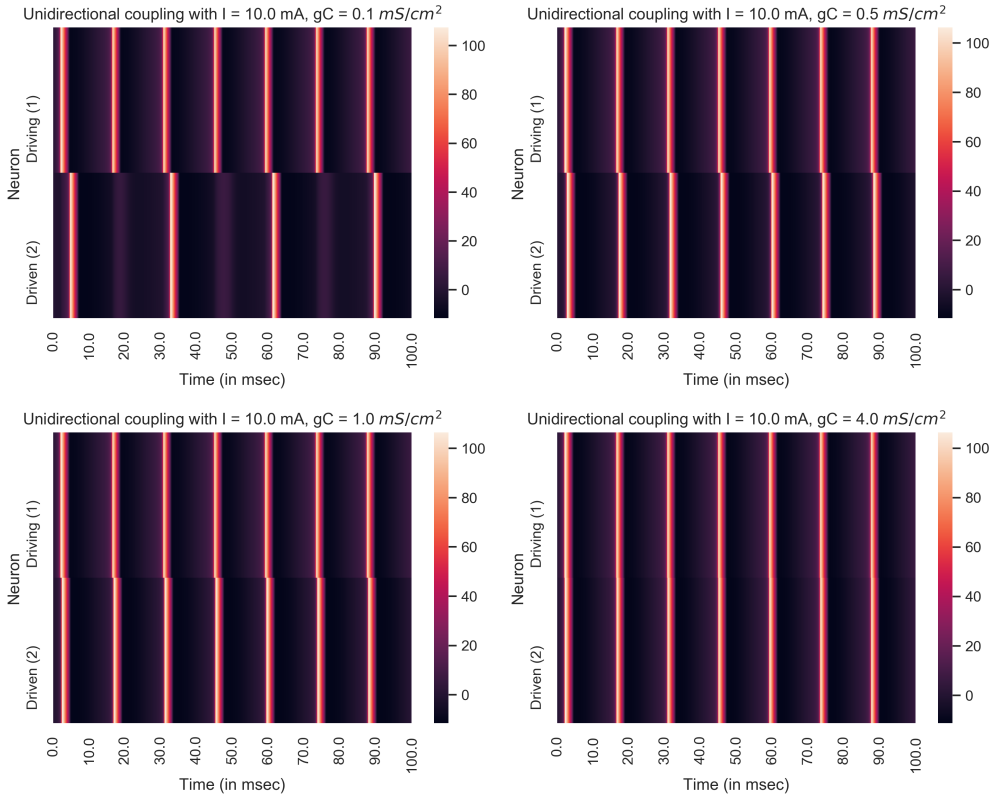

Figure 4.4: Space-time plots for increasing g_C value show shift from an asynchronous state to phase synchronization to complete synchronization. Row 1: g_C = 0.1 $\frac{mS}{cm^2}$, g_C = 0.5 $\frac{mS}{cm^2}$, and Row 2: g_C = 1.0 $\frac{mS}{cm^2}$, g_C = 4.0 $\frac{mS}{cm^2}$. Colour bar shows the voltage of action potentials.

It can be seen that for a particular input current and type of coupling (unidirectional), the synchronization increases for increase in the g_C value. At extremely low values of g_C, the neurons are asynchronized. At slightly higher g_C, the two neurons spike continuously, but

with a constant phase difference between the two. Here, they are **phase synchronized**. At higher g_C, the two neurons' spikes overlap completely and both are in **complete synchronization**.

Apart from performing the qualitative analysis of synchronization using space-time plots, we use the Synchronization Order Parameter (R), described in subsection 2.3.3, as a quantitative measure of synchronization. Figure 4.5 illustrates the evolution of complete synchronization with g_C values using R (Synchronization Order Parameter), which takes a value of unity when the action potentials of the two neurons overlap completely. It can be seen from Figure 4.5 that R increases with g_C value. It starts with a value of 0.5 and goes up to 1.0 around $g_C = 3.0 \frac{mS}{cm^2}$.

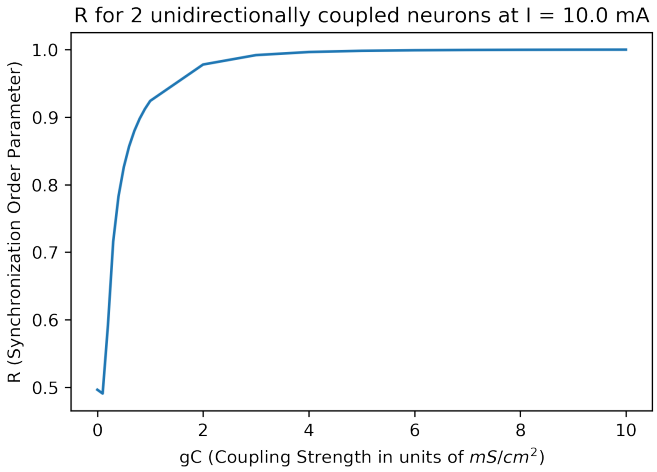

Figure 4.5: Synchronization order parameter at different g_C values for two unidirectionally coupled neurons for input current $I = 10.0$ mA in driving neuron 1.

Bidirectional coupling

The space-time plots for input current of 10.0 mA in the driving neuron 1 for bidirectional coupling are given in Figure 4.6. As has been shown earlier, in bidirectional coupling, both neurons affect each other through exchange of their electrical activities when $g_C > 0$.

Both neurons send current to each other due to bidirectional coupling.

It can be seen from all the given figures (Figure 4.6, Figure 4.7, Figure 4.8) that for a particular input current and type of coupling (bidirectional), the synchronization increases for an increase in the g_C value.

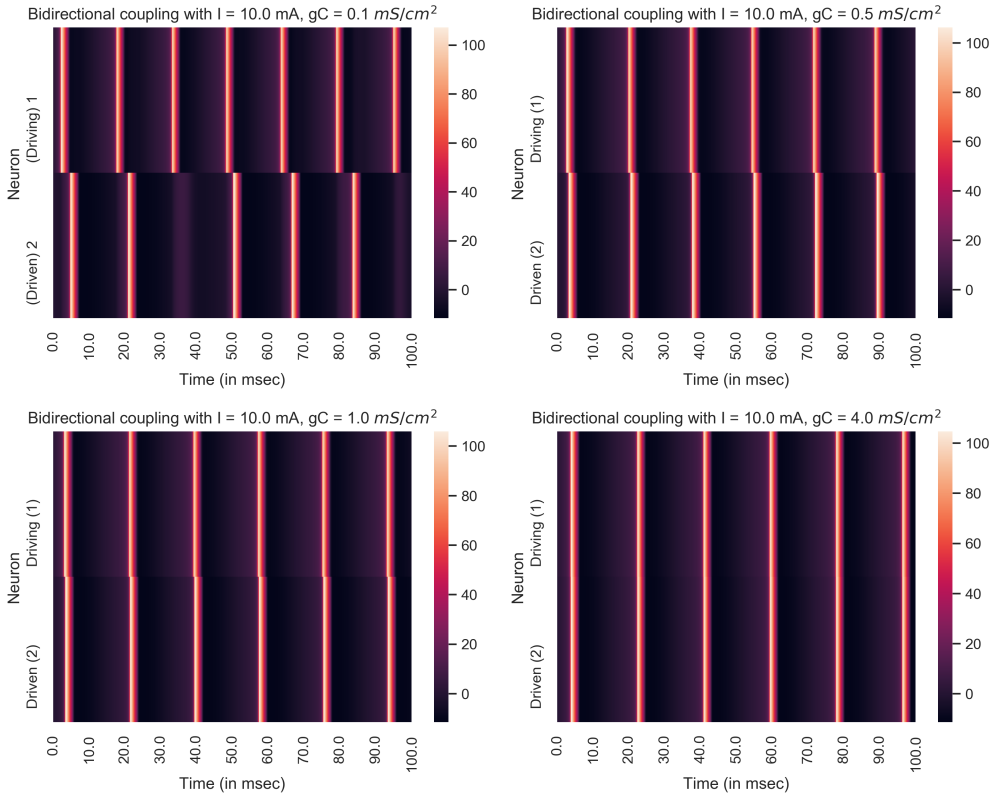

Figure 4.6: Space-time plots for increasing g_C value show shift from an asynchronous state to phase synchronization to complete synchronization. Row 1: $g_C = 0.1\ \frac{mS}{cm^2}$, $g_C = 0.5\ \frac{mS}{cm^2}$, and Row 2: $g_C = 1.0\ \frac{mS}{cm^2}$, $g_C = 4.0\ \frac{mS}{cm^2}$. Colour bar shows the voltage of action potentials.

Looking at the time series for the two neurons gives a better idea of the type of synchronization and how it develops with changing g_C values.

The first figure shows the time series for $g_C = 0.1\ \frac{mS}{cm^2}$. At this value of coupling strength, we do not even get phase synchronization. At $g_C = 0.2\ \frac{mS}{cm^2}$ (not shown here) we get phase synchronization. The amplitudes of the two do not overlap. Upon increasing the g_C value further, the oscillations overlap and the synchronization shifts from phase synchronization to complete synchronization. At $g_C = 4.0\ \frac{mS}{cm^2}$, we have almost identical time series, which is a feature of complete synchronization. We can estimate the g_C value at which the type of synchronization shifts from phase to complete synchronization from the R plot, which is given in Figure 4.8. The plot illustrates the evolution of the synchronization with g_C value quantitatively using the Synchronization order parameter (R). Looking at the graph acquired by plotting the quantitative estimate of synchronization (R) against g_C values, we confirm the qualitative result. Additionally, we can notice that the slope is steeper for bidirectional coupling. We get value of $R = 1.0$ at $g_C = 2.0\ \frac{mS}{cm^2}$ in bidirectional coupling for two

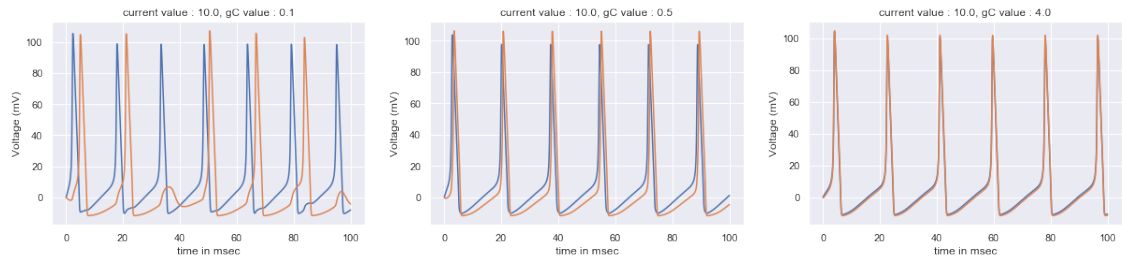

Figure 4.7: Time series from Left to Right : g_C = 0.1 $\frac{mS}{cm^2}$, g_C = 0.5 $\frac{mS}{cm^2}$, g_C = 4.0 $\frac{mS}{cm^2}$. The type of synchronization changes from no synchronization to phase synchronization to complete synchronization.

neurons at input current 10.0 mA. This suggests that bidirectional coupling makes it easier for two neurons to synchronize. They synchronize at lower g_C values. This observation also matches with frequency synchronization results.

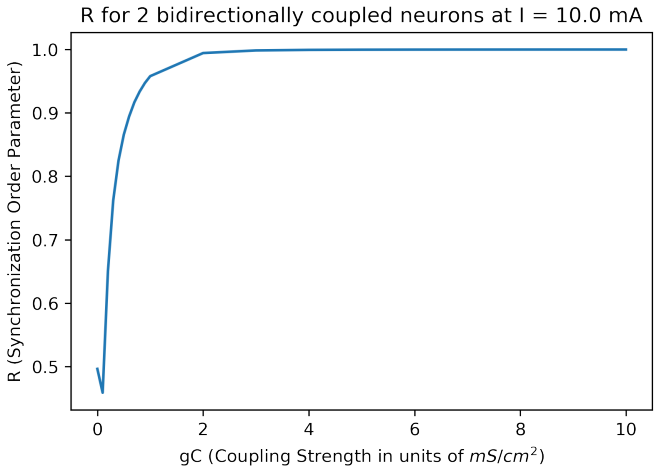

Figure 4.8: Synchronization order parameter at different g_C values for two bidirectionally coupled neurons and with input current, $I = 10.0mA$ in driving neuron 1.

4.2.2 Other Input currents in driving neuron (25.0 mA and 50.0 mA)

Unidirectional coupling

Figure 4.9 (for I = 25.0 $\frac{mS}{cm^2}$) and Figure 4.10 (I = 50.0 $\frac{mS}{cm^2}$) confirm that increasing g_C, results in a shift from an asynchronous state to phase synchronization first and later to complete synchronization for all input current values (in driving neuron 1) in the case of unidirectional coupling between the two neurons. The activity of the two neurons gets more synchronized with increased coupling strength.

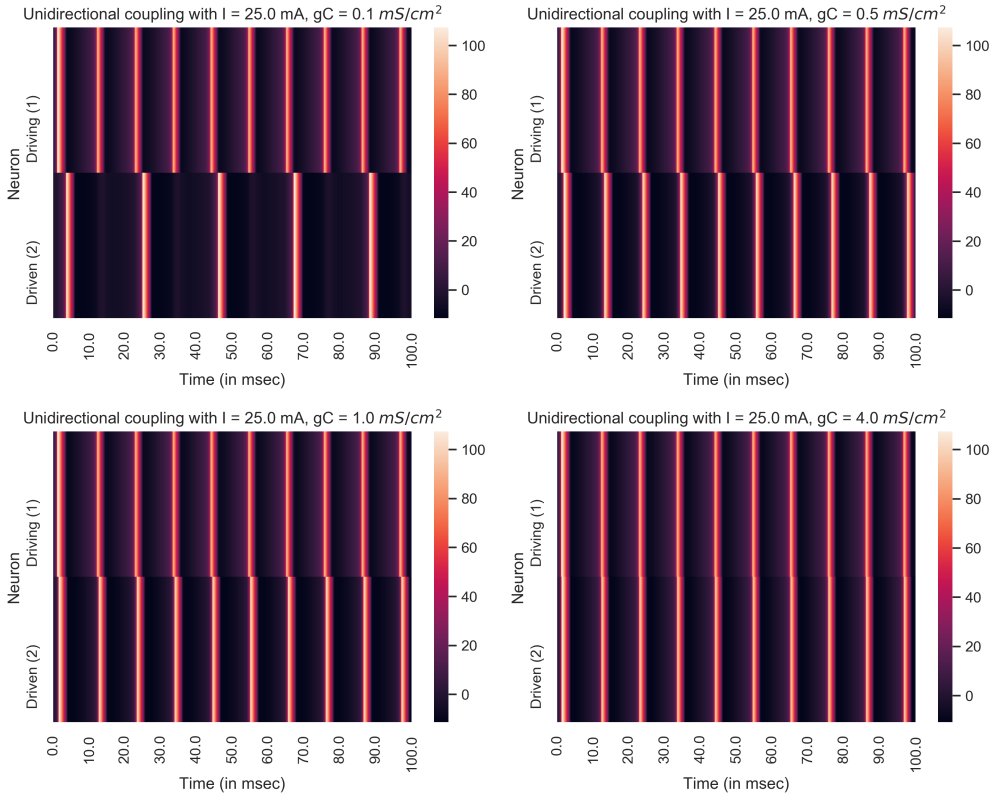

Figure 4.9: Space time plots for Input current in driving neuron 1 as 25.0 mA and type of coupling as unidirectional. Row 1: g_C = 0.1 $\frac{mS}{cm^2}$, g_C = 0.5 $\frac{mS}{cm^2}$, and Row 2: g_C = 1.0 $\frac{mS}{cm^2}$, g_C = 4.0 $\frac{mS}{cm^2}$. Colour bar shows the voltage of action potentials.

Figure 4.11 clearly illustrates the effect that the input current in driving neuron 1, has on synchronization in the two unidirectionally coupled neurons. It is seen that for unidirectional coupling, higher input currents in driving neuron 1 result in lower slopes of the g_C vs. R plot. The transition from phase synchronization to complete synchronization occurs at a higher g_C value for higher values of input current in driving neuron 1 (I). Thus, a clear result that we obtain from looking at Figure 4.11 is that a higher input current in driving neuron 1 makes it harder to synchronize two unidirectionally coupled neurons.

Bidirectional coupling

Figure 4.12 (I = 25.0 $\frac{mS}{cm^2}$) and Figure 4.13 (I = 50.0 $\frac{mS}{cm^2}$) indicate that the shift from an asynchronous state to phase synchronization and subsequent shift from phase synchronization to complete synchronization on increasing coupling strength (g_C) occurs for all values of input current in driving neuron 1 (I) in a bidirectionally coupled two neuron system.

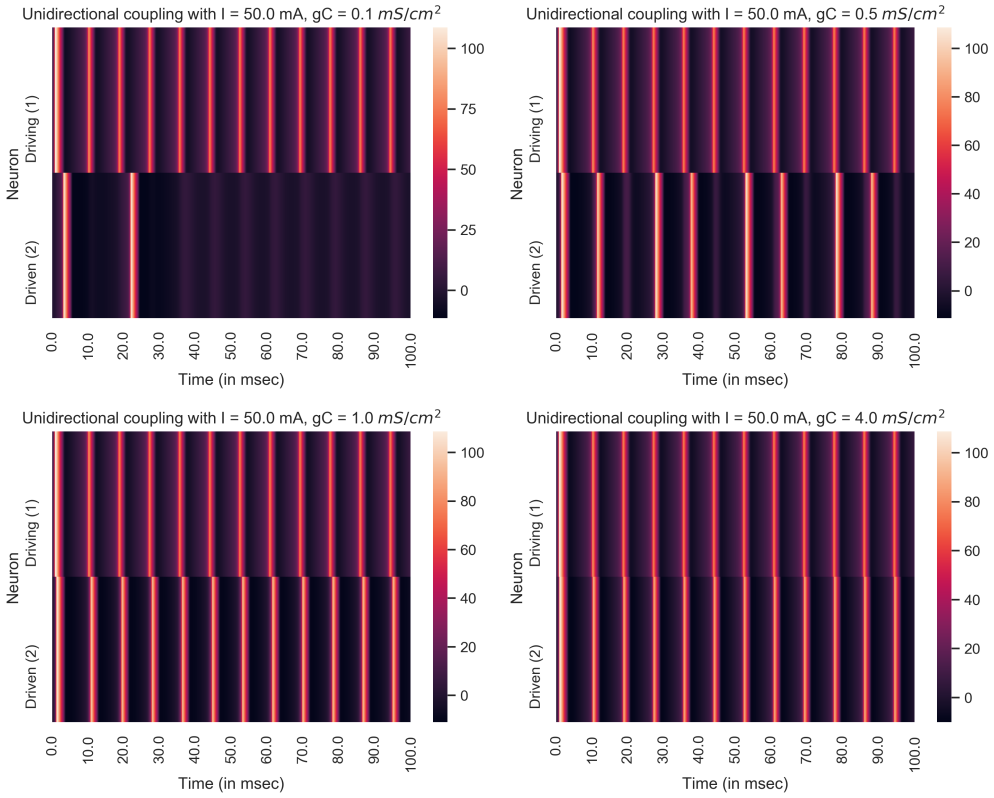

Figure 4.10: Space time plots for Input current in driving neuron 1 as 50.0 mA and type of coupling as unidirectional. Row 1: $g_C = 0.1\ \frac{mS}{cm^2}$, $g_C = 0.5\ \frac{mS}{cm^2}$, and Row 2: $g_C = 1.0\ \frac{mS}{cm^2}$, $g_C = 4.0\ \frac{mS}{cm^2}$. Colour bar shows the voltage of action potentials.

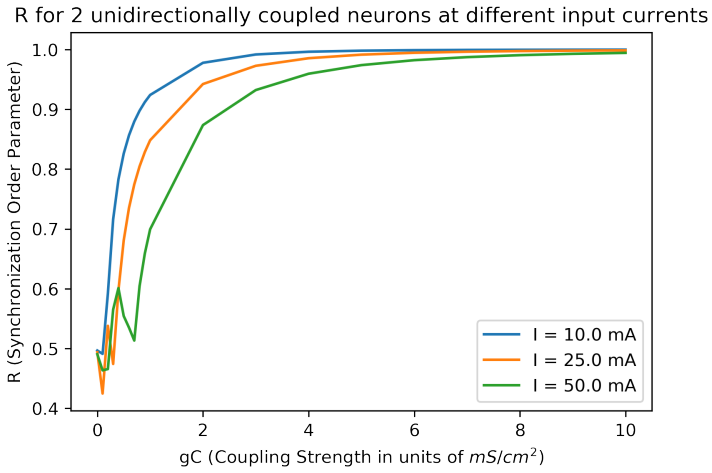

Figure 4.11: Synchronization order parameter at different g_C values for two unidirectionally coupled neurons. Different colours indicate different values of input current in the driving neuron 1.

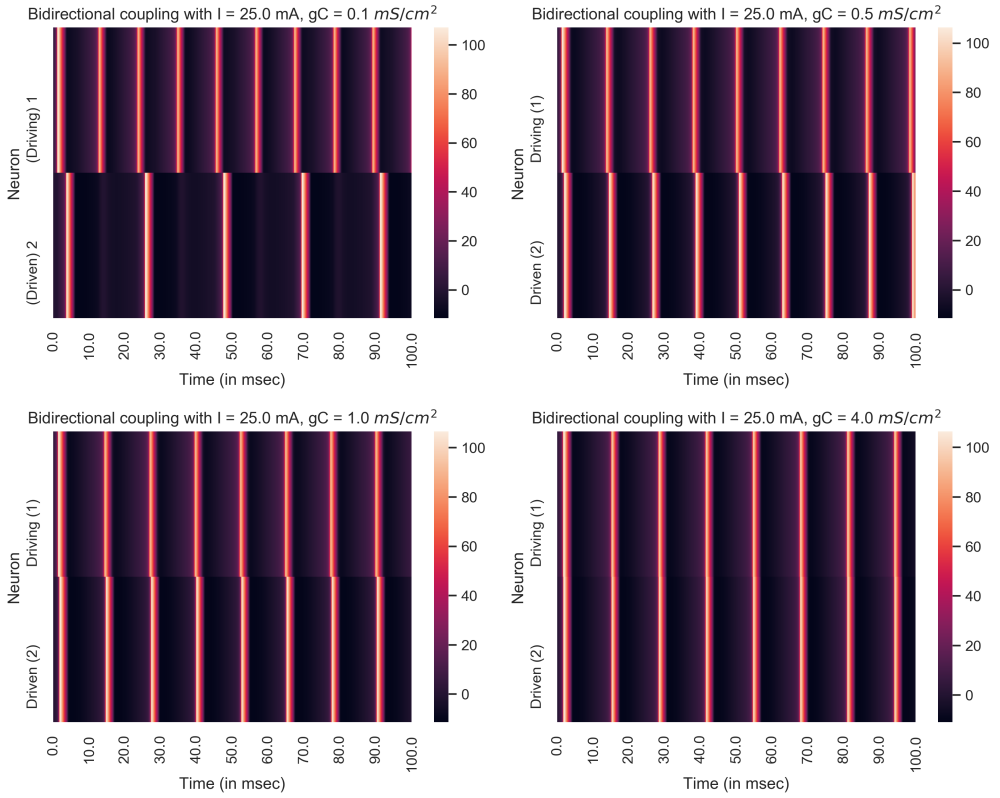

Figure 4.12: Space time plots for Input current in driving neuron 1 as 25.0 mA and type of coupling as bidirectional. Row 1: g_C = 0.1 $\frac{mS}{cm^2}$, g_C = 0.5 $\frac{mS}{cm^2}$, and Row 2: g_C = 1.0 $\frac{mS}{cm^2}$, g_C = 4.0 $\frac{mS}{cm^2}$. Colour bar shows the voltage of action potentials.

Figure 4.14 quantitatively depicts the effect that input current in driving neuron 1 (I) has on the evolution of synchronization. It is seen that a higher input current in the driving neuron 1 (I) results in a lesser R vs g_C slope, indicating that it is more difficult to synchronize two bidirectionally coupled neurons when the value of driving current is higher.

Upon comparing Figure 4.14 to Figure 4.11, it is inferred that bidirectional coupling results in an easier synchronization as compared to unidirectional coupling. This can be ascertained by comparing the slopes of the R vs. g_C plot for each of the I values in Figure 4.11 to the slopes of R vs. g_C of the corresponding I values in Figure 4.14. The slope of increase of R vs g_C value is higher for the bidirectional coupling for all values of input current in the driving neuron 1 (I = 10.0 mA, 25.0 mA and 50.0 mA respectively) than the corresponding slope in the unidirectional coupling case. The value of R reaches close to 1 for the bidirectional coupling at a lower g_C value when compared to the corresponding input current in the unidirectional case. These results further confirm the results obtained in section 4.1.

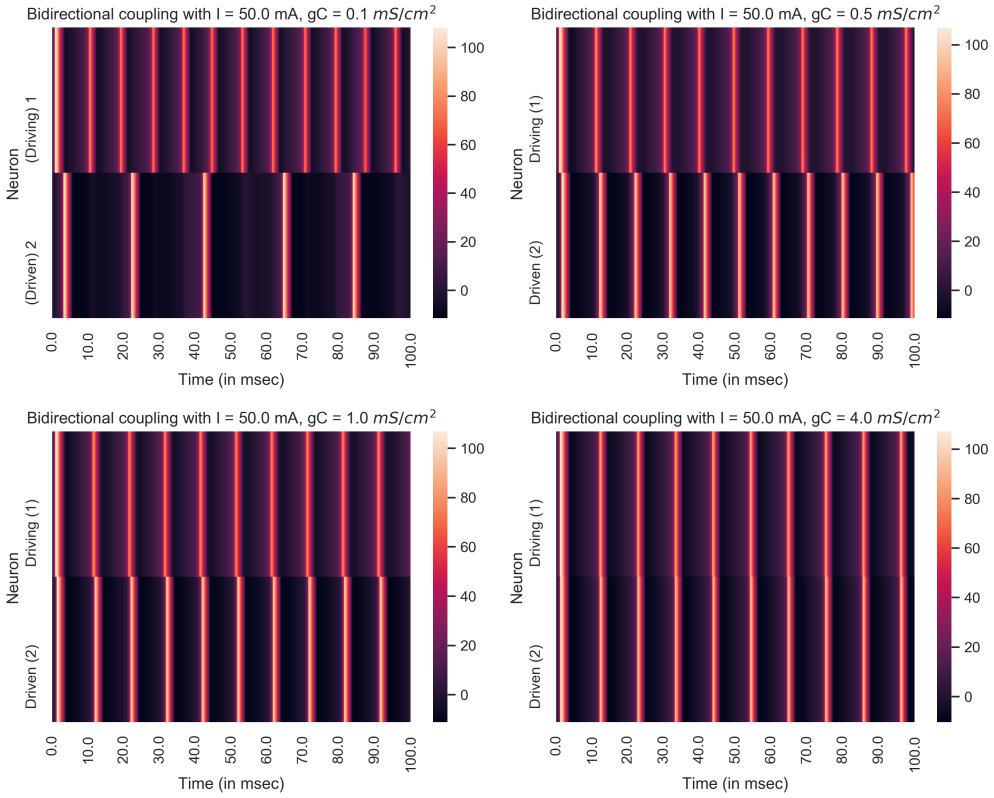

Figure 4.13: Space time plots for Input current in driving neuron 1 as 50.0 mA and type of coupling as bidirectional. Row 1: $g_C = 0.1$ $\frac{mS}{cm^2}$, $g_C = 0.5$ $\frac{mS}{cm^2}$, and Row 2: $g_C = 1.0$ $\frac{mS}{cm^2}$, $g_C = 4.0$ $\frac{mS}{cm^2}$. Colour bar shows the voltage of action potentials.

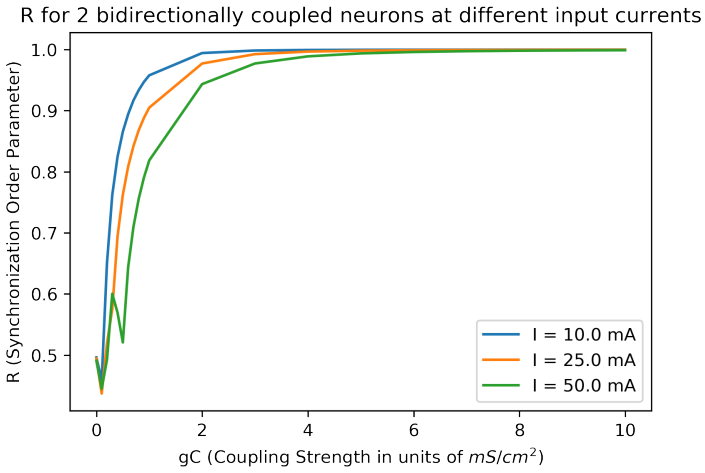

Figure 4.14: Synchronization order parameter at different g_C values for two bidirectionally coupled neurons. Different colours indicate different values of input current in the driving neuron 1.

4.3 Summary

The results in this chapter show how synchronization evolves with different parameters in a two-neuron circuit. We used other values of input current (75mA, 100mA, etc.), and the trend for those is similar to what we have observed so far. The synchronization value increases with increasing g_C, and it decreases with increasing input current in the driving neuron. A comparison of phase synchronization in unidirectional and bidirectional coupling indicates that bidirectional coupling results in synchronization at lower g_C. The fact that bidirectional coupling leads to better synchronization in two neurons is further seen in Figure 4.15 below. This figure depicts the value of g_C at which phase synchronization occurs in two unidirectional and bidirectionally coupled neurons for different input currents in the driver neuron. This points out to the value of g_C needed for a particular input current in the driving neuron and how this value changes by changing input current value for both unidirectional coupling and bidirectional coupling. The blue line is for unidirectional coupling, and the orange line is for bidirectional coupling. The unidirectional coupling plot has a higher slope, indicating that for a certain input current in the driving neuron, higher g_C values are required to generate synchronization of the two neurons. Interestingly, the line separating regions marked by phase synchronization to no phase synchronization in the g_C-I parameter plane for bidirectional coupling is linear. However, for unidirectional coupling, it deviates from linearity. It might be due to a higher symmetry present in the bidirectional coupling case.

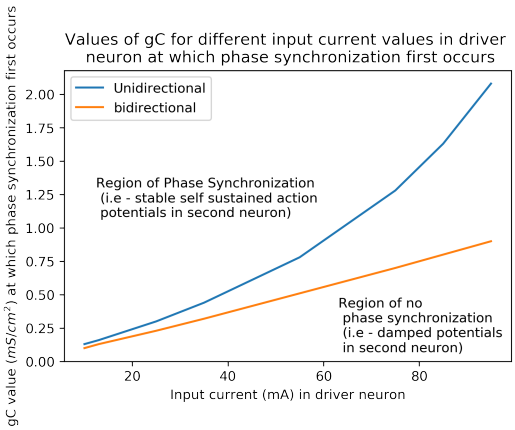

Figure 4.15: Dependence of phase synchronization on the input current in neuron 1 (I) in unidirectional (Blue line) and bidirectionally (Orange line) coupled neurons, shown in the g_C-I parameter space.

Chapter 5

Dynamics of Multiple Coupled Neurons on Variation of Parameters

This chapter continues the study of probing the dynamics and synchronization properties in networks (rings and chains) of multiple electrically coupled neurons. The effects of parameters, I and g_C, are analyzed for these larger networks of coupled neurons. The overall results obtained in the case of two neurons, remain primarily unchanged even for higher number of neurons. However, with increased number of neurons, the additional parameters whose effect on synchronization was probed included - (i) Network length, and (ii) Boundary conditions (Periodic - Ring and Fixed - Chain). The focus of the results given here would be to highlight the effect of these parameters on synchronization and transmission of information in multiple coupled neurons, while also discussing the effect of parameters studied earlier (I, g_C and Coupling type).

The HH equations for multiple electrically connected neurons are very similar to the ones in the two neuron case. There is an input current in the first neuron. This neuron sends current through the electrical synapse to the next connected neuron and so on. The two types of arrangements studied for multiple neurons are the **unidirectional chain** and the **bidirectional ring**. The unidirectional chain arrangement is such that the neurons on the two ends of the chain are not connected (Fixed boundary conditions), and the coupling type between all the neurons is unidirectional, with neuron 1 being the driving neuron with input current. The bidirectional ring arrangement of n neurons has periodic boundary conditions, so each neuron (say i^{th} neuron) in this arrangement is connected to exactly two neurons - to the $(i+1)^{th}$ and $(i-1)^{th}$ - and follow bidirectional coupling. Here also the neuron 1 is

the driving neuron, but it connects to both the 2^{nd} and the n^{th} neurons electrically.
Due to the high computational complexity, we had to limit our simulations to 50 neurons with each neuron represented by four nonlinear coupled HH equations. We also did a few simulations for 100 neurons, but these take a lot of time. In order to study networks of larger sizes, higher computational power is needed. Simulations were done for network sizes of 3, 5, 10, 25, and 50 neurons. We have presented results for the 5, 10, and 50 neuron cases and used these to arrive at general results for network lengths in the range mentioned above.

5.1 Case 1: Five neurons

5.1.1 Unidirectional chain

In unidirectional chain arrangement, the first neuron gets a constant input current (I=50 mA), and communicates with the second neuron unidirectionally, with the help of the electrical synapse, which is then one-way coupled to the third neuron, and so on. The fifth neuron gets the input current from the fourth neuron and it can not pass it any further. The results for a five unidirectionally coupled chain of neurons are discussed below and given in Figures 5.1 and 5.2.

- Figure 5.1 reveals that the electrical activity of each neuron in the chain sets up with increasing phase difference with respect to neuron 1, due to the increased delay in receiving current from the previous neurons. At lower g_C, less current is transferred, and the spike frequency is lesser than the driving neuron. The space time plots show a wave-like electrical activity along the chain that travels from the first neuron to the final neuron. At higher g_C values, the phase difference between the neurons keeps decreasing and all neurons spike at the same frequency due to increased $I_{electrical}$. This is an indicator of better synchronization at higher coupling strength.

- The quantitative assessment with Figure 5.2 using the synchronization order parameter (R) reveals that the system attains close to complete synchronization (i.e.- $R = 1.0$) at around $g_C = 18.0\ \frac{mS}{cm^2}$.

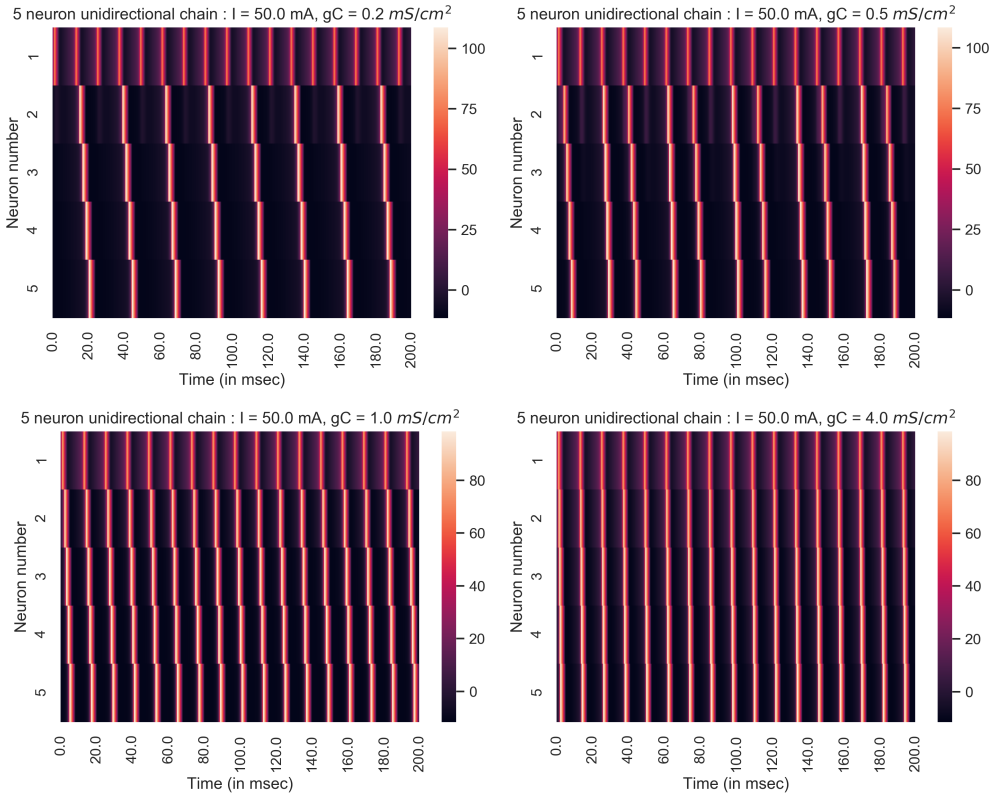

Figure 5.1: Space-time plots for increasing g_C value for 5 neurons unidirectional chain. Row 1: $g_C = 0.2\ \frac{mS}{cm^2}$, $g_C = 0.5\ \frac{mS}{cm^2}$, and Row 2: $g_C = 1.0\ \frac{mS}{cm^2}$, $g_C = 4.0\ \frac{mS}{cm^2}$.

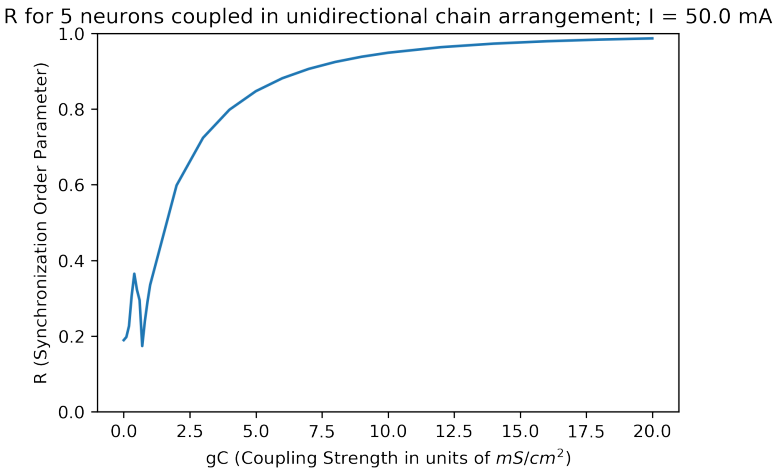

Figure 5.2: Synchronization order parameter at different g_C values for five unidirectionally coupled neurons in chain arrangement with I = 50.0 mA

Note that we have studied g_C values up to 20.0 $\frac{mS}{cm^2}$ for 5 neurons, because complete synchronization values are achieved only at high g_C values for larger networks with higher number of neurons. Comparing the synchronization order parameter, R, for the 5 neurons

case (Figure 5.2) to the two neurons case (Figure 4.5) for unidirectional coupling, it is observed that the slope is less and the R = 1.0 value (complete synchronization) is achieved at a much higher g_C value here. Thus, increasing the number of neurons while keeping other conditions similar makes it difficult to synchronize the network.

5.1.2 Bidirectional ring

As described earlier, the bidirectional ring arrangement allows electrical coupling of each neuron to both the adjacent neurons. Thus, both neuron 2 and 5 are now driven directly by the driving neuron 1.

The figures to illustrate the collective dynamic behaviour of the five bidirectionally coupled ring of neurons are given in Figures 5.3 and 5.4.

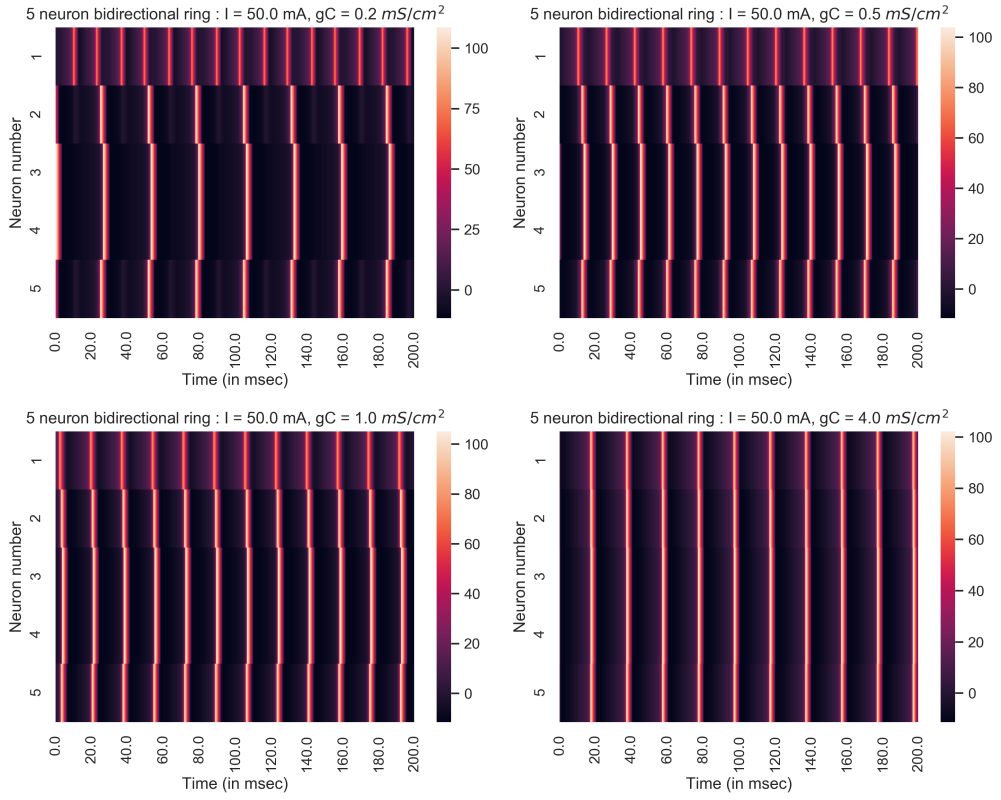

Figure 5.3: Space-time plots for increasing g_C values for 5 neuron bidirectional ring. Row 1: $g_C = 0.2\ \frac{mS}{cm^2}$, $g_C = 0.5\ \frac{mS}{cm^2}$, and Row 2: $g_C = 1.0\ \frac{mS}{cm^2}$, $g_C = 4.0\ \frac{mS}{cm^2}$.

- The space time plots (Figure 5.3) show that, since the signal travels both ways in a ring, the second and the fifth neuron fire in perfect synchrony. Similarly, the third and the fourth neurons behave in a synchronous fashion (even for extremely small values

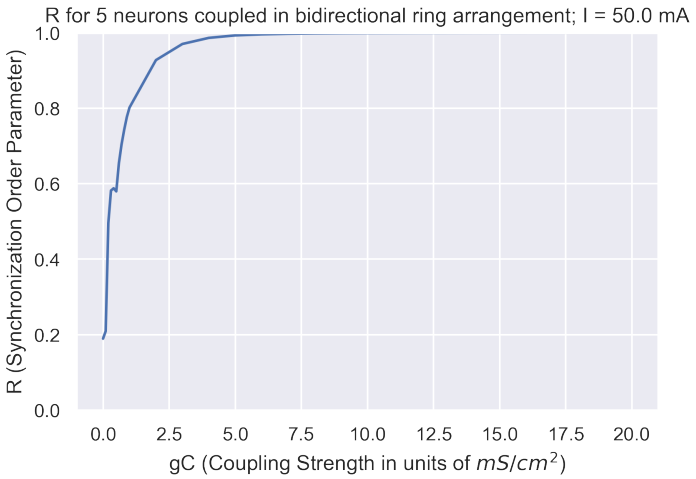

Figure 5.4: Synchronization order parameter at different g_C values for five bidirectionally coupled neurons in ring arrangement with I = 50.0 mA.

of coupling strength (g_C)). As the whole circuit is symmetrical about the first neuron, it is expected that the firing pattern should be synchronous about that neuron. Of course, like in the previous case, increasing the g_C value synchronizes these neurons more and the lag decreases upon increasing g_C values.

- Synchronization order parameter (R) plot in Figure 5.4 is similar to that of the two neuron case - showing that the bidirectional ring of five neurons is synchronized at much lower gC value compared to the uni-directional chain of five neurons (Figure 5.2). The value of R is close to 1.0 at $g_C = 3.0\ \frac{mS}{cm^2}$ and it quickly touches 1.0 at around $g_C = 5.0\ \frac{mS}{cm^2}$. Our results show that a ring-like network of neurons with bidirectional coupling is better for synchronization than a unidirectional chain-like arrangement.

Note that similar to the two coupled neurons case, there is a negative effect of increasing the input current value on synchronization for the five neurons case. This was ascertained with both space time plots and the study of the Synchronization order parameter. As the effect of input current on synchronization was discussed in length for the two neurons case in Chapter 4, and because the effect remains the same for higher number of neurons, we have not explicitly shown results for varying input currents for these larger network sizes.

5.2 Case 2: Ten neurons

5.2.1 Unidirectional chain with I as 50.0 mA

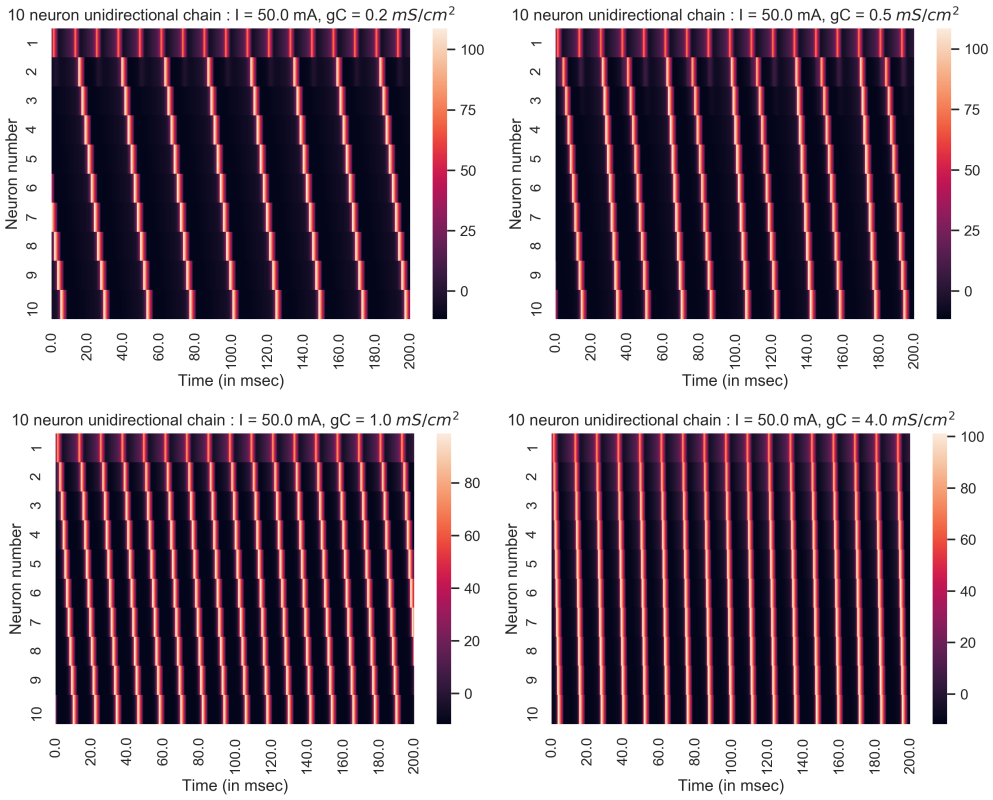

Figure 5.5: Space-time plots for increasing g_C value for 10 neuron unidirectional chain. Row 1: g_C = 0.2 $\frac{mS}{cm^2}$, g_C = 0.5 $\frac{mS}{cm^2}$, and Row 2: g_C = 1.0 $\frac{mS}{cm^2}$, g_C = 4.0 $\frac{mS}{cm^2}$.

Space-time plots in Figure 5.5 show a wave like pattern which travels from the first to the tenth neuron and synchronization is seen to increase with increased coupling strength (g_C). Figure 5.6 shows that the value of R reaches around 1.0 only at g_C values as high as 20.0 $\frac{mS}{cm^2}$. The slope for R $vs.$ g_C is lesser for ten unidirectionally coupled neurons (Figure 5.6) when compared to five unidirectionally coupled neurons (Figure 5.2). These results further confirm the results discussed in Section 5.1 that increasing the number of neurons makes it more difficult to synchronize them.

5.2.2 Bidirectional ring with I as 50.0 mA

Figure 5.8 indicates that the value of R reaches very close to 1.0 around $g_C = 10.0$ $\frac{mS}{cm^2}$. It further increases and almost touches 1.0 at around $g_C = 12.0$ $\frac{mS}{cm^2}$. Since complete

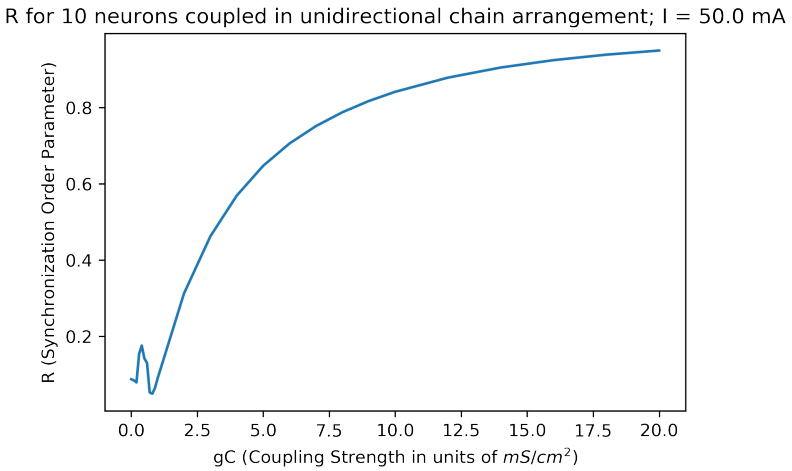

Figure 5.6: Synchronization order parameter at different g_C values for ten unidirectionally coupled neurons in chain arrangement with I = 50.0 mA.

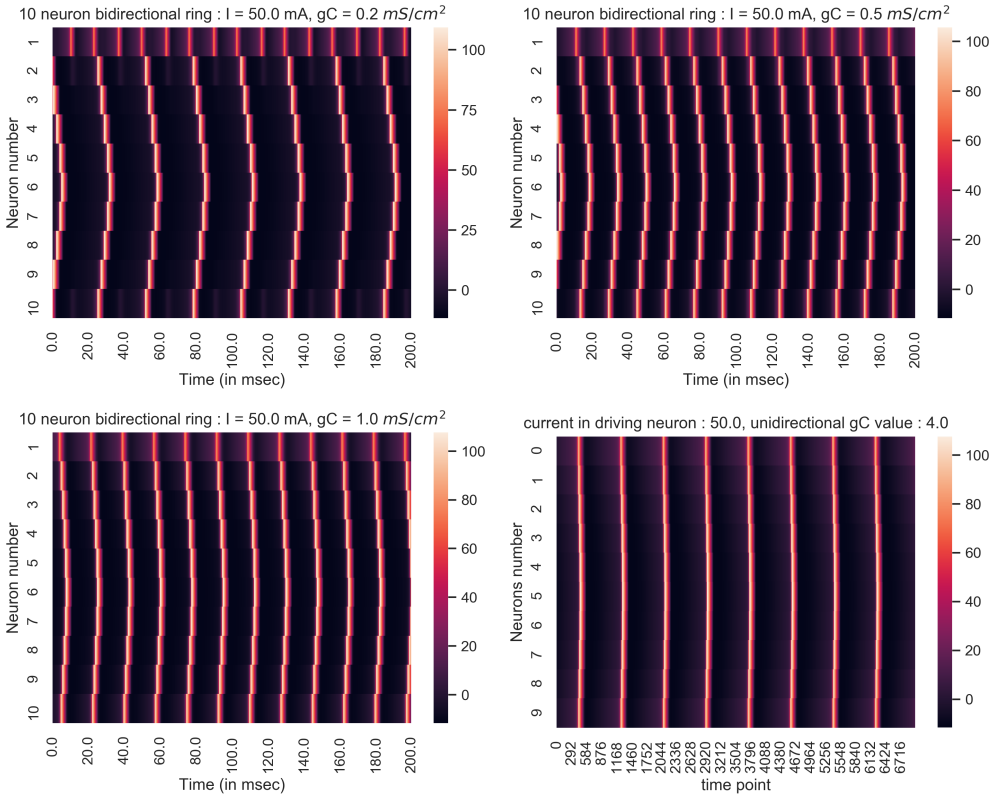

Figure 5.7: Space-time plots for increasing g_C value for 10 neuron bidirectional ring. Row 1: $g_C = 0.2\ \frac{mS}{cm^2}$, $g_C = 0.5\ \frac{mS}{cm^2}$, and Row 2: $g_C = 1.0\ \frac{mS}{cm^2}$, $g_C = 4.0\ \frac{mS}{cm^2}$.

synchronization (R = 1.0) is attained at a lower g_C value for bidirectional ring arrangement in 10 neurons as compared to unidirectional chain, this confirms that a bidirectional ring of 10 neurons offers better synchronization than a unidirectional chain of 10 neurons.

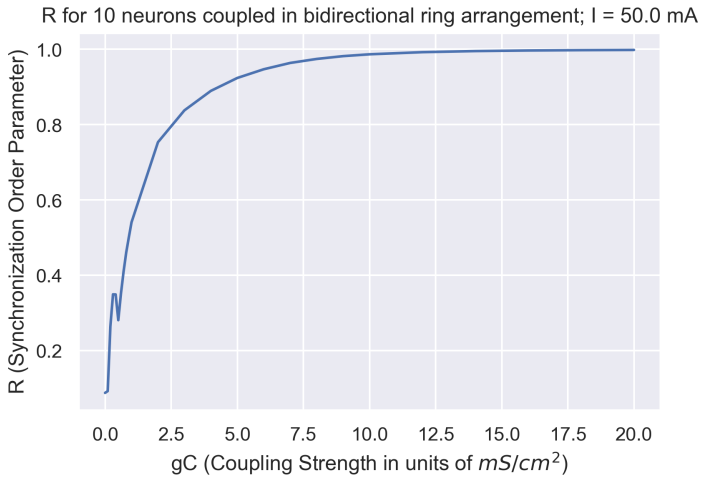

Figure 5.8: Synchronization order parameter at different g_C values for ten bidirectionally coupled neurons in ring arrangement with I = 50.0 mA.

5.3 Case 3 : Fifty neurons

It is seen that a bidirectional ring is not always better for synchronization than the unidirectional chain in case of network length of 50 neurons. Thus, the results for 50 neurons are presented in three subsections. In subsection 5.3.1 and 5.3.2, we have compared the unidirectional chain with the bidirectional ring results of 50 neurons with 50.0 mA input current with the help of the Synchronization Order parameter. The R value of 1.0 is attained at a lower g_C value for the unidirectional chain as compared to the bidirectional ring. Whether this is an anomaly that only occurs at higher input current values (50.0 mA) or whether a similar pattern is observed for all input currents in the 50 neurons case is explored in subsection 5.3.3, where we see results for comparatively lower input currents (10.0 mA and 25.0 mA) for the 50 neurons case.

5.3.1 Unidirectional chain with I as 50.0 mA

Figure 5.10 illustrates that the value of R does not reach 1.0 even for values of g_C as high as 20.0 $\frac{mS}{cm^2}$. As plotting the R value against g_C values requires running a "for-loop" for very small increments in g_C, it takes a lot of time and computational power and so, we could not plot the R vs g_C plot for higher g_C values (for the 50 neurons case). However, we managed to ascertain the value of g_C for which R reaches very close to 1.0 (by selecting g_C using trial and error). It is found that an R value of 0.99 is attained around a g_C value of 250 $\frac{mS}{cm^2}$

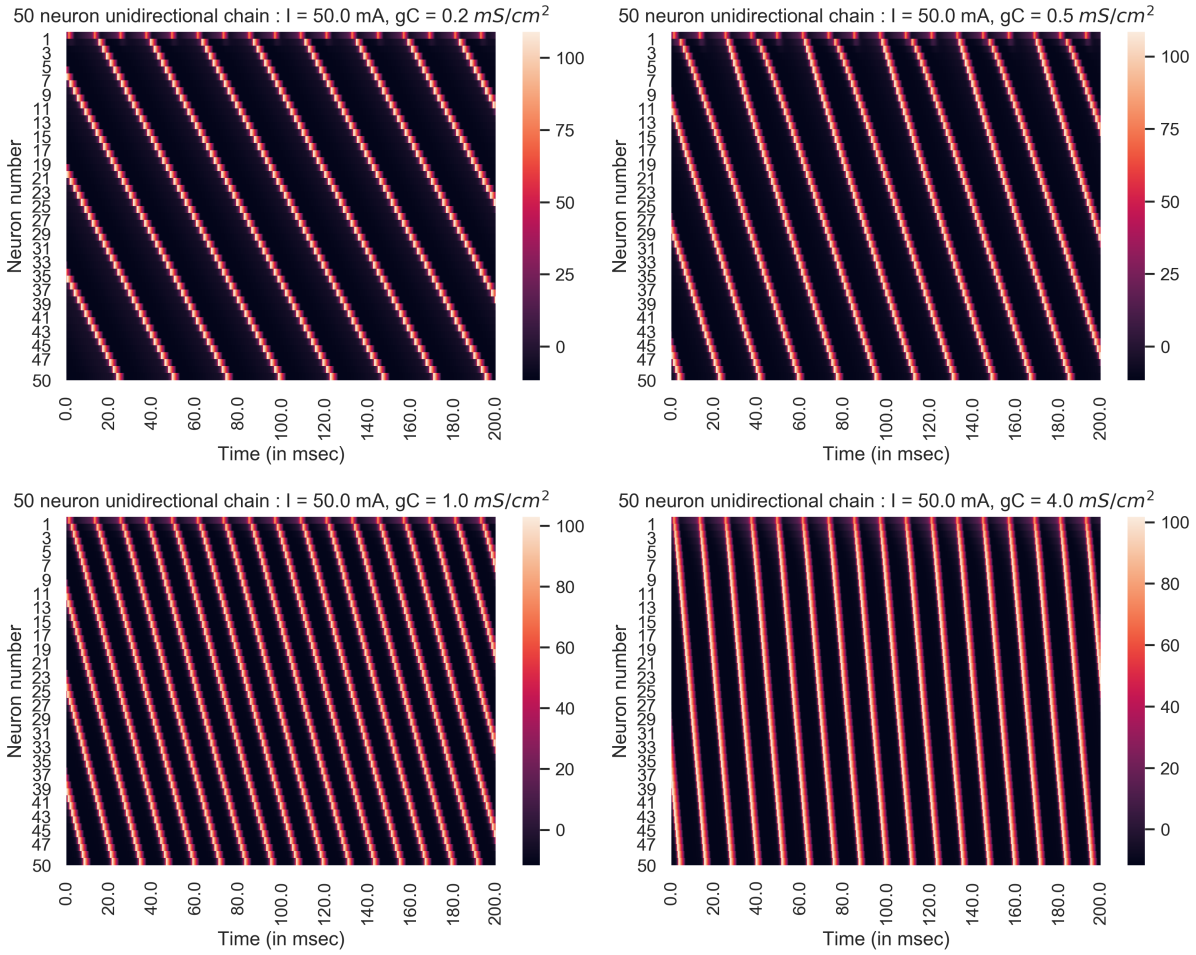

Figure 5.9: Space-time plots for increasing g_C value for 50 neuron unidirectional chain. Row 1: $g_C = 0.2\ \frac{mS}{cm^2}$, $g_C = 0.5\ \frac{mS}{cm^2}$, and Row 2: $g_C = 1.0\ \frac{mS}{cm^2}$, $g_C = 4.0\ \frac{mS}{cm^2}$.

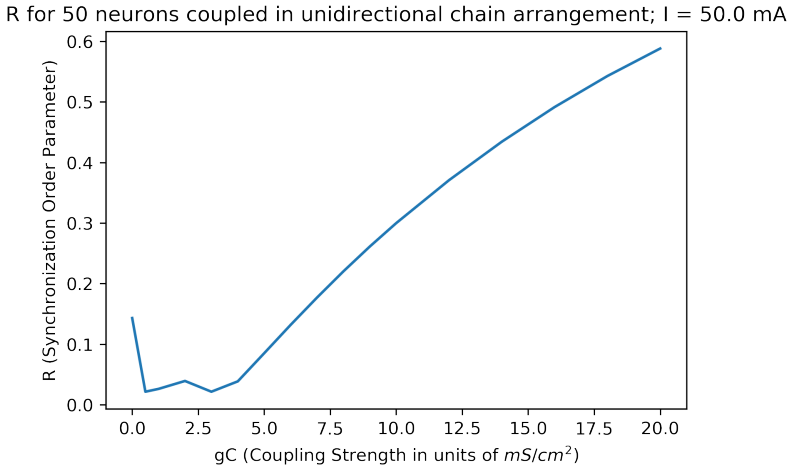

Figure 5.10: Synchronization order parameter at different g_C values for fifty unidirectionally coupled neurons in chain arrangement with I = 50.0 mA.

5.3.2 Bidirectional ring with I as 50.0 mA

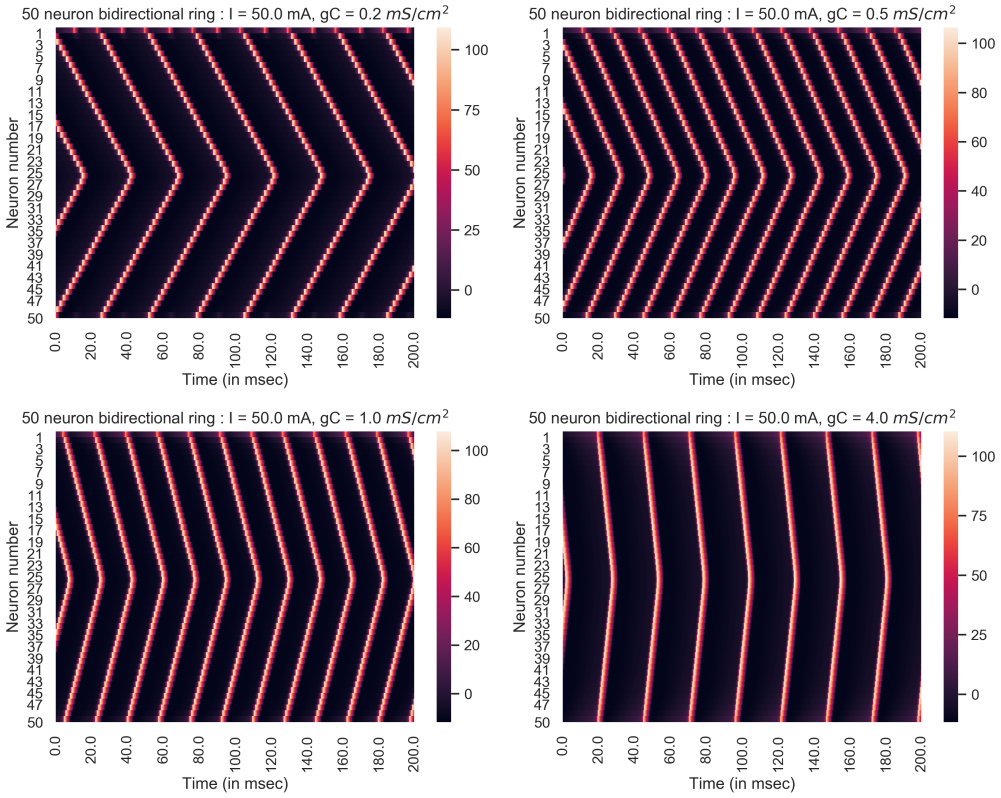

Figure 5.11: Space-time plots for increasing g_C value for 50 neuron bidirectional ring. Row 1: $g_C = 0.2\ \frac{mS}{cm^2}$, $g_C = 0.5\ \frac{mS}{cm^2}$, and Row 2: $g_C = 1.0\ \frac{mS}{cm^2}$, $g_C = 4.0\ \frac{mS}{cm^2}$.

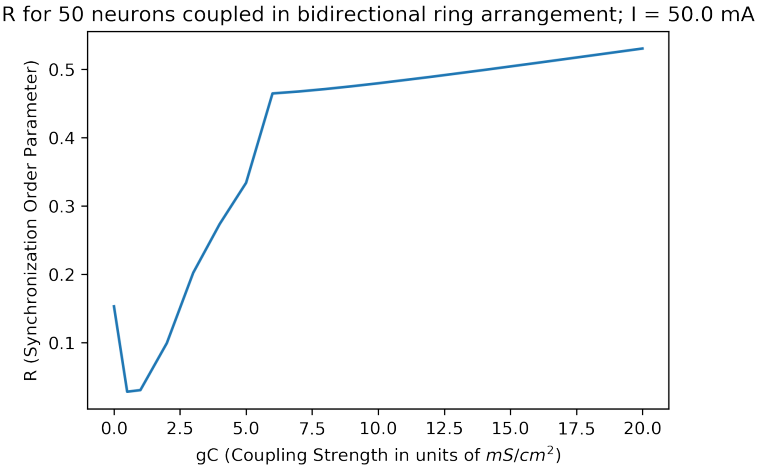

Figure 5.12: Synchronization order parameter at different g_C values for fifty bidirectionally coupled neurons in ring arrangement with I = 50.0 mA

Figure 5.12 illustrates that the value of R does not reach 1.0 till $g_C = 20.0\ \frac{mS}{cm^2}$ even for

bidirectional coupling in ring arrangement for 50 neurons. The slope increases really fast at first till R reaches 0.5 and then the slope decreases to a very low value. In fact, the value of R = 0.99 is reached at a very high g_C value of around 650 $\frac{mS}{cm^2}$. This value of g_C at which complete synchronization is attained for a bidirectional ring of 50 neurons is much higher than the g_C value required in the case of a unidirectional chain of 50 neurons. Thus, these results indicate that a unidirectional chain of 50 neurons is better for synchronization than a bidirectional ring when input currents are high (50.0 mA). This suggests that for higher number of neurons (around 50), there might be a more complex dynamics at work for synchronization, and we cannot simply state that a bidirectionally coupled ring is always better than a unidirectionally coupled chain of neurons for all the input currents simulated when the number of neurons is around 50. We still need to carry out more simulations with 50 neurons to completely rule out all the other possibilities for such a result (for example - the presence of a longer transient in case of higher network lengths which needs to get removed before evaluating the Synchronization Order parameter) and accepting that this sort of a dynamics is seen in higher network sizes. Along with this, we need to run a few more simulations for network sizes greater than 50 neurons to understand the dynamics at play for larger networks. The simulations require significantly more computational time to complete as the number of neurons increase. We have discussed this at length along with a discussion on future perspectives for modelling multiple coupled neurons in the Discussion chapter (Chapter 7). However, results for other input current values and boundary conditions for 50 neurons are presented in subsection 5.3.3 to paint a better picture of what could be ascertained from simulations done so far.

5.3.3 Other results for 50 neurons

Figure 5.13 has four images depicting the evolution of R (Synchronization order parameter) with coupling strength (g_C) for different input currents in a 50 neuron unidirectional chain and bidirectional ring. It can be seen that for the 50 neuron bidirectional ring case, even at these lower input current values (10.0 mA and 25.0 mA), a bend in the R vs g_C curve is seen (seen in the bottom images in Figure 5.13). The value of R seems to reach a limiting value and then grows very slowly after that. The bend in the curve is seen at a lower R value for higher input currents. This is not the case for unidirectional coupling where the curve for R versus g_C is continuous. Apart from that, we evaluated the value of g_C at which

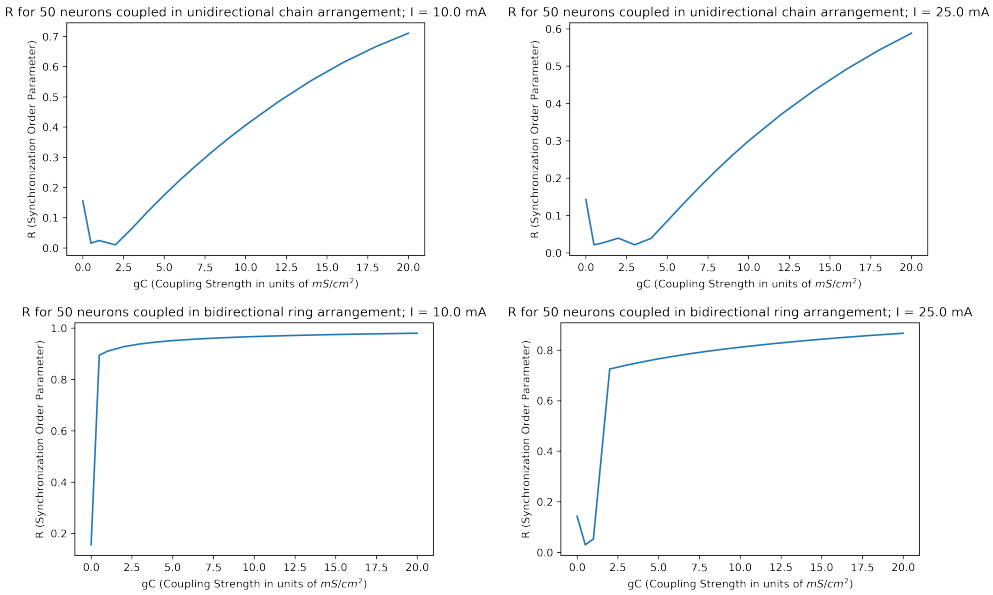

Figure 5.13: Evolution of the synchronization order parameter with g_C for different input current values and boundary conditions in 50 neurons. The upper two graphs are for unidirectional chains and the lower ones are for bidirectional rings. The figures on the left are for 10.0 mA current while those on the right are for I value as 25.0 mA

complete synchronization (R = 1.0) is achieved. These values are :-

1. For the unidirectional chain of 50 neurons with input current 25.0 mA, the value of R = 0.99 is achieved at around the value of $g_C = 150\ \frac{mS}{cm^2}$. However, for the bidirectional ring, the value of R = 1.0 is achieved at a higher g_C value of 180 $\frac{mS}{cm^2}$. This difference in the g_C values is not as high as in the 50.0 mA input current case discussed in the previous two subsections. However, even in this case, it implies that a unidirectional chain is better than a bidirectional ring of 50.0 mA input current when the current is 25.0 mA.

2. For the unidirectional chain of 50 neurons with input current 10.0 mA, the value of R = 0.99 is achieved at around the value of $g_C = 90\ \frac{mS}{cm^2}$, and for the bidirectional ring, the value of R = 1.0 is achieved at a lower g_C value of 45 $\frac{mS}{cm^2}$. Thus, for these lower values of input currents, the usual results that the bidirectional ring is better for synchronization than a unidirectional chain still hold.

Three possibilities emerge from this observation - (i) Higher network sizes obey a more complex dynamics for synchronization, (ii) Only higher network sizes with high input cur-

rent values obey a complex dynamics of synchronization and the usual results of bidirectional ring being better for synchronization than the unidirectional chain are valid otherwise, and (iii) The results for the case of 50 neurons were an anomaly. These could be ascertained by modelling higher network sizes at different input currents values(e.g., 100 neurons). We also wish to point out that up until now, a transient of 60 msec was removed from a time series of 200 msec to evaluate R. We need to test these results with longer time ranges and upon removing a longer transient as this might have an effect on the results. This was not possible up until now due to the limited computational power available. Similarly, other simulations mentioned above with higher network sizes need to be carried out to make conclusive statements about the dynamics at play for higher network lengths. Thus, in conclusion, all the other results (effect of input current, effect of number of neurons etc. on synchronization) hold for both smaller and larger network sizes. However, even though we know for sure that a bidirectional ring is better than a unidirectional chain for smaller network sizes, there might be a few exceptions to this particular result as we go to higher network lengths. A set of conclusions for the results obtained so far on the synchronization of coupled neurons are presented in the Summary section.

5.4 Summary

The conclusions for multiple coupled neurons are summarized below:-

1. Synchronization increases with increasing coupling strength (g_C values).
2. Increasing the number of neurons makes it more difficult to synchronize the network.
3. Increasing the input current in driving neuron makes it difficult to synchronize the network.
4. Bidirectional ring arrangement provides better synchronization than Unidirectional chain arrangement at least for lower network sizes.
5. More simulations are to be done for higher network sizes (50 neurons and more) to conclusively highlight the difference between the synchronization ability of the unidirectional chain and the bidirectional ring in larger networks.

Chapter 6

Estimating Parameters from Neuronal Activity using Bayesian Inference

The final aspect of the work deals with an inverse approach to parameter analysis. This work is at a preliminary stage. Rather than generate the output variable by simulating a deterministic model after feeding the parameters, they are estimated from experimental data. In real neurons and neuronal circuits, the individual and emergent action potentials generated are under many other influences (internal or external to the system), which contribute to add stochasticity or noise to the measurement of the voltages (say, in single neuron action potentials, or EEG, ECG, etc.) [26]. In this chapter we explore the methods employed to study the time series of noisy measurements (neuronal output voltage here) to estimate parameters of a known mathematical model (such as, the Hodgkin-Huxley model of neurons). Many probabilistic estimation methods exist in Statistics and this section considers only the methods used for the Bayesian paradigm. The studies made in this area consist of learning about the Bayesian methods and preparing noisy datasets from the HH equations for future studies.

Various approaches for Bayesian estimation of parameters exist. Section 6.1 deals with the review of the literature and discussion of various preexisting algorithms for Bayesian Inference of parameters. Section 6.2 deals with simulation of the Hodgkin Huxley model with different types of noise introduced to the output to generate noisy HH data. The final aim is to then apply the Bayesian techniques in parameter estimation discussed in section 6.1 to noisy data, which is generated according to the protocol followed in section 6.2. This would help in gaining a better understanding of the effects of different types of noises on

the parameter estimation algorithms. This is an important aspect because different biological sources can interact to produce processes containing different types of noises in them. Thus, to summarise, we give techniques in Bayesian inference followed by Hodgkin Huxley model plots with different underlying noise distributions. The final aim is to combine these two aspects and understand the effectiveness of the numerical techniques in parameter estimation for different noise types.

6.1 Concepts in Bayesian Inference

6.1.1 Bayes' theorem

Probability theory consists of two approaches. The first one being the frequentist approach [27], and the second one being the Bayesian approach [28]. The basis of the Bayesian approach to probability lies in Bayes' theorem [28], which states that the probability of an event keeps updating with observation (new incoming data). There are four key variables which make up the mathematical formula for the Bayes' theorem. These are -

1. The posterior probability - The posterior probability is the newly updated probability once new data is observed.

2. The prior probability - The probability of an event occurring before new data is observed.

3. The likelihood - The likelihood is the probability of observing the new data, given that the event occurred.

4. The evidence - Evidence is obtained from all the data present. It is the probability of the preexisting data. It acts as a normalizing constant in the formula for the Bayes' theorem.

The following is the mathematical formula for the Bayes' theorem:-

$$P(parameter|data) = \frac{(P(data|parameter)) \times P(parameter)}{P(data)} \tag{6.1}$$

- Posterior probability = ((Prior probability)$\times$(likelihood))/(Evidence)

This is the Bayes' theorem, which gives us the rules for updating of probabilities with data.

6.1.2 Algorithms in Bayesian Inference

A few algorithms used in Bayesian Inference are highlighted in this subsection. Each of these algorithms has different advantages and disadvantages.

Markov Chain Monte Carlo methods (MCMC algorithms)

These are a group of methods that use Markov chain processes with a Monte Carlo sampling technique [29, 30]. A Markov chain is a stochastic process that does not have long-term memory. This means that in a Markov chain process, the next state is only dependent on the previous state. A Monte Carlo sampling technique samples with a defined probability distribution. The sampling is done from a set of randomly generated numbers coming from a given probability distribution. These two together govern the selection criteria in MCMC processes.

Monte Carlo integration draws samples from the given distribution and then approximates averages as expectation values. An MCMC algorithm draws from these samples by running a Markov chain for a long time. Following are a few algorithms that follow this approach.

- Metropolis Hastings Algorithm [31, 32]- The classic algorithm which is most used from the MCMC methods.

- Hamilton Monte Carlo algorithm [33]- This algorithm looks at the sampling from a physical analogy and relies on the application of theoretical concepts from classical mechanics to solve the problem. It is faster than the Metropolis Hastings algorithm.

- Gibbs sampling method [34]- This is a simplification (special case) of the Metropolis Hastings algorithm.

MCMC algorithms do not need the evidence term (in Eq. 6.1) for the calculation of the posterior probability. This is really advantageous because the numerical estimation of the evidence term is often infeasible. Thus, these methods are particularly useful when the evidence is not known.

Likelihood Free Inference/ Approximate Bayesian computation

As the name suggests, this numerical technique does not require the Likelihood variable in the Bayes' formula for updating probabilities for purposes of parameter estimation. Approximate Bayesian Computation is a type of Likelihood Free Inference method for Bayesian Inference [35]. ABC (Approximate Bayesian Computation) requires the following:-

1. Data.
2. Generative model to generate data.
3. Prior.
4. Criteria for when the simulated data matches the actual data.

The following are the steps for carrying out Approximate Bayesian computation:-

1. The preexisting data is used to evaluate the parameters like mean etc. which gives us a prior probability distribution for the parameter values.
2. From this distribution, parameter values are taken out and simulations are performed.
3. Probability distributions for the parameter values are evaluated for each of the simulation and then, based on a threshold for tolerance, it is decided whether these simulations generate data sufficiently close to the observed data and data is updated.
4. This gives us a posterior estimate.

Other uses of ABC may be in model comparison. Limitations of ABC include the following.

- Small number of models used to estimate posterior due to high computational cost
- High dimensionality may require a large number of parameters to be estimated, and thus, a large number of simulations may be required (Computational complexity).

Approximate Bayesian Computation is particularly useful when a Likelihood function is not available or computationally infeasible/ expensive to evaluate. This method may be implemented with software like PyABC or the abc R package.

Variational inference

This algorithm frames parameter estimation as an optimization problem. This is a faster and computationally scalable algorithm and this acts as an advantage in certain cases.

Many numerical implementation of the above-mentioned algorithms exist in literature and as libraries in Python and other software tools.

6.2 Data generation for parameter estimation

Biological processes are not as precise as the deterministic mathematical models that we used to simulate them. Action potential generation in real biological systems are never as deterministically regulated as given by the plots obtained from the simulation of the coupled non linear equations in the Hodgkin Huxley model. The Hodgkin Huxley model, in fact, represents the ideal behaviour in biological systems where there is no stochasticity present. Real biological processes have noise in them. Besides, the noise in these biological systems could originate from different types of probability distributions and be both white and coloured [36]. Parameter estimation in real neuronal systems would thus have to overcome the difficulties posed by the presence of noise - both in parameters and variables. In this section, as the simplest case, we simulate the Hodgkin Huxley model by introducing additive noise in the output voltage at every integration step. We give below simulation results for the Hodgkin Huxley model with noise introduction in it. Figure 6.2 illustrates three types of random distributions which are used to simulate noise which is then fed into the Hodgkin Huxley model. The simulation results and the corresponding histograms are shown for HH model - (a) With Gaussian random noise, (b) Noise from Poisson distribution, and (c) Noise from Uniform distribution respectively. Note that for illustration purposes, the mean and variance for all three types of input noise given in Figure 6.2 are taken equal to 3.0 mV. Figure 6.1 represents a simulation of the HH neuron without any input noise. This is given for purposes of comparison.

The future prospects are to apply the numerical methods in Bayesian Inference discussed in Section 6.1 for parameter estimation in noisy signals with different types of background noise (as given in Figure 6.2 as illustration).

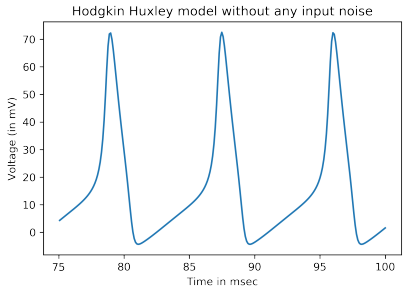

Figure 6.1: HH neuron for parameter values : $\bar{g}_{Na} = 120.0\ \frac{mS}{cm}$ and $\bar{g}_K = 36.0\ \frac{mS}{cm}$ and I = 50.0 mA for with no input noise

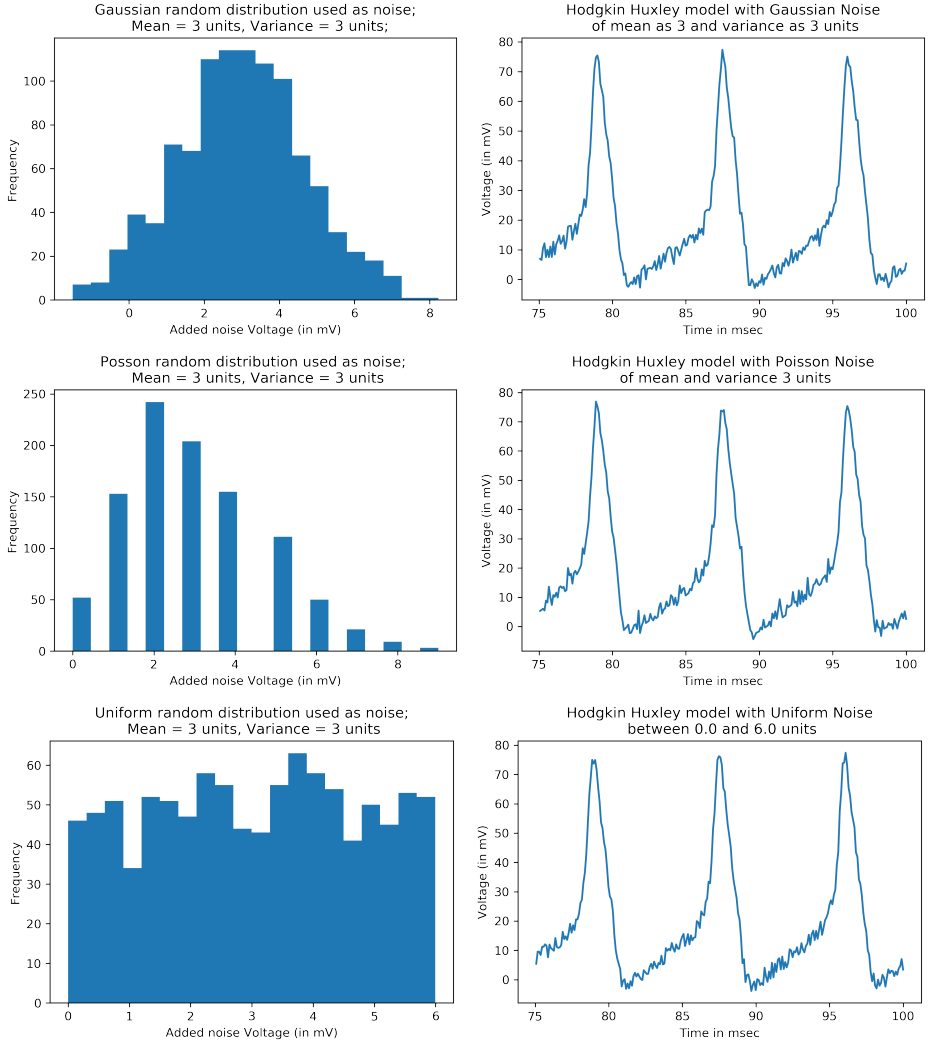

Figure 6.2: (Left) : Histograms for Gaussian random distribution, Poisson random distribution and Uniform random distribution used for generating (Right) : Plots generated for Hodgkin Huxley model for Gaussian random noise, Poisson random noise and Uniform random noise respectively. Parameter values are $\bar{g}_{Na} = 120.0\ \frac{mS}{cm}$ and $\bar{g}_K = 36.0\ \frac{mS}{cm}$ and I = 50.0 mA

Chapter 7

Summary and Outlook

Neurons act as messengers of information in living systems with action potentials acting as the messages. The action potential arises from various ion channel (specifically, sodium and potassium) activities interacting at different scales, which are successfully modelled by the four-variable Hodgkin-Huxley (HH) equations. The coordinated activity of single and networks of neurons make it possible for living organisms to perform their cognitive functions. The two most important features of this electrical activity are the frequency and amplitude of the emergent oscillations of action potentials from the neuronal networks. This study explores the functioning of a neuron as a dynamical system, and the role that various electrical parameters play in the singular and coordinated activity of neurons. The three broad categories of work are :-

1. Mapping the electrical parameter space of ion channel conductance and input currents ($\bar{g}_K, \bar{g}_{Na}, I$) of the Hodgkin Huxley single neuron and highlighting the properties of transitions in dynamic behaviours.

2. Understanding the effect of various parameters in driving synchronization in networks of neurons of different sizes coupled through gap junction coupling (electrical synapse).

3. Bayesian Inference techniques for parameter estimation in noisy HH model.

These three together, complete a study of the analysis of parameters in the HH neurons by bringing together the methods of computational modelling and data analysis. The first two points highlight the role of parameters in driving the dynamic activity (of output voltage) of single and coupled neurons, while the third point emphasises on a reverse approach to

obtain the parameters when the data on the output voltage is given. In this chapter, we summarize and further elaborate on some of the results obtained so far. Section 7.1 summarizes single neuron results and highlights different ways of looking at the transitions in the dynamics in parameter space. Section 7.2 summarizes coupled neuron results and highlights the future perspectives of computational modelling of coupled neurons. Finally, there are a few anomalies encountered in the results obtained so far and section 7.2 highlights those as well.

7.1 Single Neuron results - Additional Perspectives

We mapped the $(\bar{g}_K, \bar{g}_{Na}, I)$ 3 dimensional parameter space of the HH neuron with the help of 2 parameter plots of the $\bar{g}_K, I$ and the $\bar{g}_K, \bar{g}_{Na}$ planes (Chapter 3). The study aimed to find the effect of these parameters on the dynamics of the action potential. It was discovered that -

1. The $(\bar{g}_K, I)$ two parameter plane (Figure 3.3) has a bounded region inside which the asymptotic dynamics behaviour of the single neuron is stable self sustained action potentials and everywhere outside, it exhibits steady state dynamics (damped potentials). The area of the enclosed region gets larger upon increasing the third parameter $(\bar{g}_{Na})$. The dynamic transitions in this plane are viewed in terms of the amplitude of oscillations of the asymptotic states.

2. The $(\bar{g}_K, \bar{g}_{Na})$ two parameter plane (Figure 3.8) consists of a region of stable self sustained action potentials that is bounded on three sides but open on the fourth. Outside this region, steady state solutions (damped potentials) exist. Boundaries of this region are approximated as straight lines. Increasing the third parameter (Input current, I) decreases the slope of the first transition boundary (from damped oscillations to stable self sustained action potentials) until it converges to a fixed value. Also, increasing the input current shifts the second boundary (from stable self sustained action potentials to damped potentials) downwards by a value proportional to the increase in the input current. In other words the value of the constant (intercept, in the equation of a line) decreases linearly with increase in input current for the second boundary of transitions.

3. The two boundaries (upper and lower) of the enclosed region in the (g_K -I) two parameter plot (Figure 3.2), showed an interesting difference in the transition dynamics from inside to outside. A neuron always exhibited self-sustained oscillations for parameters in the inside region, and the asymptotic dynamics was fixed point for parameters at the outside. The nature of change in dynamics, on changing parameters, is different along the two boundaries. Simulations show that in the lower boundary (orange points) from damped oscillations to self sustained action potentials, the spike amplitude of the oscillations rises abruptly as parameters are closer to the first boundary, whereas near the upper boundary (blue set of points) this is not seen, and sustained oscillations reduced to damping oscillations very gradually for some values of g_K and abruptly for other g_K values on crossing the boundary.

Below, we give two perspectives with which one could examine the transitions in dynamic behaviour in the $\bar{g}_K, I$ parameter plane. In the results given in Chapter 3, these transitions were computed numerically, and viewed in terms of the variation of the amplitude of oscillations upon transition, which is elaborated in point 3 above. In that light, these results can be interpreted from two perspectives as given down below : -

1. **Bifurcation perspective** - Stability analysis of HH equations are prohibitively difficult. Thus, obtaining these boundaries from stability analysis to denote changes in stability characteristics of the HH equations from unstable (limit cycle) to fixed point (outside) in the two-parameter plots is rather difficult. Yet, rather than trying to ascertain properties based on the amplitude of oscillation, if we try to focus along the I-axis for a fixed value of $\bar{g}_K$ and $\bar{g}_{Na}$, we can view this result in terms of bifurcations. To illustrate this, we notice that at smaller I values, one gets asymptotic steady state dynamics with damped oscillations. Linear stability analysis should give a stable fixed point here. Upon increasing the input current, the steady state loses its stability, and bifurcates on crossing the boundary into a region of unstable steady state solutions marked by large amplitude oscillations (Stable self sustained action potentials) as seen by the orange points in Figure 3.2. At the other boundary, on increasing the I-value still further, the system shows reverse-bifurcation from unstable steady state to the fixed point state with damped oscillations dynamics (blue points in Figure 3.2). Whether the transition of going back to the steady state solution is through gradual or abrupt change, in the amplitudes of oscillation, is dictated by the $\bar{g}_k$ value at fixed

value of $\bar{g}_{Na}$. This is a classic example of bifurcation happening in a low dimensional (single neuron) system. The plots in Figure 7.1 schematically represent the dynamics of change in amplitude of sustained oscillations in the two boundaries at bifurcation using the blue region.

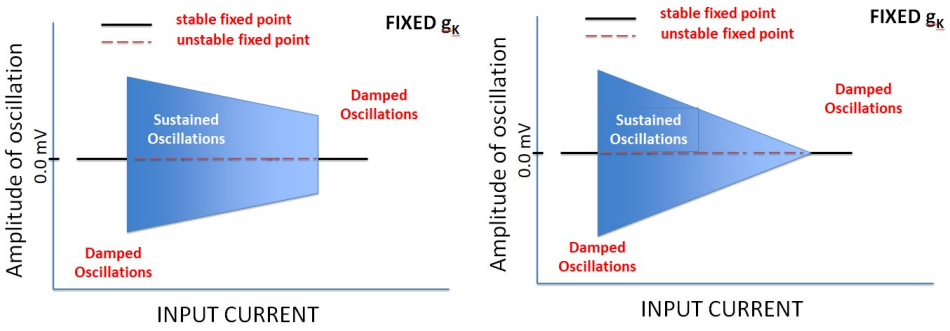

Figure 7.1: Schematic for the bifurcation perspective: (Left) - $\bar{g}_K < 10.0$, where increasing I results in abrupt increase in amplitude of oscillation at the lower boundary (orange set of points in Figure 3.2) and an abrupt decrease in amplitude of oscillations at the upper boundary (blue set of points in figure 3.2); (Right) - $\bar{g}_K \geq 10$, where increasing I results in abrupt increase in amplitude of oscillation at the lower boundary (orange set of points in Figure 3.2) and then further increasing the I results in a gradual and continuous decrease in amplitude of oscillation at the upper boundary (blue set of points in Figure 3.2) for value of $\bar{g}_{Na} = 120.0\ \frac{mS}{cm^2}$. The dark line outside the blue region in both graphs representing stable fixed points also represents zero amplitude of oscillations.

Bifurcation theory is usually the accepted nomenclature in the context of explaining and understanding the dynamics of stable-unstable transitions in low dimensional dynamical systems. Figure 7.1 gives a schematic perspective of looking at the single neuron results through the lens of bifurcation dynamics. This is the widely accepted theory of looking at low dimensional dynamical systems.

2. **Phase Transitions perspective** - Here we show that the theory of phase transitions could be another way of viewing these results. We give the phase transition perspective of looking at these results for single neuron dynamics. If we view the amplitude of oscillations as an order parameter and try to classify the transitions into either first order phase transitions or continuous phase transitions, we note that transitions accompanied by an abrupt change in the order parameter are referred to as first order

phase transitions, and transitions accompanied by a gradual and continuous change in the order parameter are referred to as continuous phase transitions. Thus, according to the results regarding amplitude mentioned above in the subsection on properties of transitions, we would label all the transitions marked by orange points in Figure 3.2 as first order phase transition. Similarly, we would label blue transition points with $\bar{g}_K < 10.0 \frac{mS}{cm^2}$ as first order transitions and those with $\bar{g}_K \geq 10 \frac{mS}{cm^2}$ as continuous transitions. Also note that usually, a first order transition is accompanied by a loss function. An example of a loss function accompanying first order transitions in states of matter is latent heat. Something similar to that could be expected in this case too. Such loss functions could be ascertained experimentally. Knowing what the loss function is, in this case, could be interesting. Along with, for the second set of transition, why does this loss function go away for $\bar{g}_K \geq 10 \frac{ms}{cm^2}$ for $\bar{g}_{Na} = 120 \frac{ms}{cm^2}$ case would also be interesting to know. We point out that even though we give an analogy with phase transitions here, it requires a deeper understanding of the phases associated to conclusively talk about phase transitions in the single neuron case. We just consider the stable self sustained action potentials as one phase and the damped potentials as the other phase. Thus, looking at these as phase transitions could be an alternative way of looking at these results.

The overall dynamics is similar even for other values of $\bar{g}_{Na}$. For example, for $\bar{g}_{Na} = 150.0 \frac{ms}{cm^2}$ also, we get all our first set of transitions as first order. Also the second set of transitions follow a similar dynamics with lower $\bar{g}_K$ values showing first order transitions while higher $\bar{g}_K$ values showing continuous phase transitions. Though this change in order of transition does not occur at $\bar{g}_K = 10 \frac{ms}{cm^2}$. It occurs at a slightly higher $\bar{g}_K$ value. The dynamics is however similar.

7.2 Multiple Coupled Neurons - Future Perspectives and Anomalies

Chapter 4 and Chapter 5 deal with the dynamics of electrically coupled neurons (uni and bidirectionally) and their ability to exhibit synchronized sustained oscillations with changing parameters when only the first neuron has Input current. The results obtained are sum-

marised below.

For two neurons:-

1. Increasing the coupling strength (g_C) leads to increased synchronization in the two neuron network. The activity shifts from asynchronous to phase synchronized and subsequently to complete synchronized activity.

2. Increasing input current makes it harder to synchronize the two neurons.

3. Bidirectional coupling between two neurons results in better synchronization than unidirectional coupling.

For multiple (more than two) neurons:-

1. Synchronization increases upon increasing the coupling strength (g_C) and the state of the network goes from asynchronized state to phase synchronized and subsequently to complete synchronization. Increasing the input current in the driving neuron 1, makes it difficult to synchronize the multiple neuron network.

2. Increasing the number of neurons makes it harder to synchronize the network.

3. The bidirectional ring offers better synchronization than a unidirectional chain. This result is always valid for small networks. Even though observation for 50 neurons have been reported in Chapter 5, the results for larger networks (50 neurons and more) can be summarised only after longer simulations on larger networks.

Below, we point out a few interesting observations for the case of multiple neurons. We also discuss future prospects and possible questions that could be answered for the dynamics of coupled neurons using a similar approach used here.

- Our results have shown that a bidirectional ring is better than a unidirectional chain for synchronization of the network. However, the precise difference in ability to synchronize a network between the ring and the chain arrangement, for a particular type of coupling (unidirectional or bidirectional), can only be ascertained by doing further simulations of bidirectional chains and unidirectional rings. However, we can state with reasonable confidence that a ring arrangement is better for synchronization that

a chain arrangement. The following is an argument supporting the premise. Upon comparing the results of a 5 neuron bidirectional ring with I = 50.0 mA (Figure 5.4) to results for two neuron bidirectional coupling with I = 50.0 mA (green line plot in 4.14), it is observed that in both cases, complete synchronization (R = 1.0) is achieved at around $g_C = 5.0\ \frac{mS}{cm^2}$. Thus, the negative effect of increasing network length in the ability to synchronize is not markedly seen here. In fact, the ring arrangement (for the 5 neurons) is nullifying or maybe even overpowering the negative effect of increasing the number of neurons on g_C values. The two topologies of connections not studied here are - the "unidirectional ring" and "bidirectional chain" arrangements. Simulations with these network structures are necessary to validate the claim with certainty, and this could be an interesting avenue of future prospects in modelling of multiple electrically coupled neurons.

- The ability of a synchronized circuit of multiple electrically coupled neurons to drive itself is another interesting aspect that could be looked into. This could be done by replacing the constant input current that is given to our multiple coupled neurons (in Chapter 4 and 5) with a step down input current which inputs a constant positive value of I to the driving neuron (neuron 1) initially, and then shut the input current off after some time interval. It would be interesting to note if the multiple neuron system continues to show sustained action potential generation after the input current is turned off. If it does, then its dependence on coupling strength (g_C) and pre-step input current value ($I_{initial}$) can be studied.

- The simulations done so far could be done for higher network sizes (requiring more powerful computing systems and longer simulation times). It would be interesting to note whether the results obtained so far hold for larger networks as well. It would also be important to then study the spatiotemporally locally stable transient dynamics that these networks will show as are seen in many realistic neural systems [37–39].

  The last point brings us to some anomalies that exist for the multiple neuron results. There are certain parametric combinations for coupled multiple neurons where stable self sustained action potentials are not sustained in coupled neurons. For example - for the combination of five neurons, bidirectional coupling, ring arrangement at 10.0 mA input current, we just get graded potentials in all neurons and stable self sustained

action potentials are not sustained for $g_C \geq 0.3\ \frac{mS}{cm^2}$. These instances of the network unable to sustain stable sustained action potentials are relatively low for input current values less that 100.0 mA though. At input current of 200.0 mA in driving neuron, the network is often not able to sustain self sustained action potentials in all connected neurons. In this thesis, work has ben done with input currents, I $\leq$ 100.0 mA, where these exceptions are rare. Thus, our generalization of results needs to be considered based on the limitations mentioned above. Besides that, another unusual result that we obtained is easier synchronization for unidirectional chain of 50 neurons with input current as 50.0 mA and 25.0 mA than the bidirectional ring case (explained in detail in section 5.3). This result needs to be tested more extensively and whether this is an anomaly or if this happens for all large networks has to be ascertained with more simulations on higher number of neurons for longer simulation times.

The Chapter 6 highlights future perspectives to this work using the Bayesian approach of parameter estimation. It may be noted that the noisy time series have been obtained by introducing stochasticity (from different distributions) to the voltage variable of the HH equations. It is also possible to have noisy parameters. There are several ways to introduce variability in the network of neurons. In this thesis, all neurons have been considered identical. But in reality each neuron may have a slightly different maximum ionic conductance or coupling strength. This also introduces heterogeneity in the system which may affect the readout voltage of the network. These can be considered in future work.

In summary, this thesis reports detailed analyses based on extensive simulations of the Hodgkin-Huxley model neurons - single and coupled networks - to study the dependence of several parameters (ion channel conductances, input current, coupling strength, topology of coupling, and network length) on the nature and synchronization potential of the action potentials. Limitations and possible discrepancies in the results have been discussed clearly, and future work that may add more understanding to these properties have also been proposed to be undertaken in the future.

Appendix A

Codes

Python 3 in Jupyter was used for computational modelling and coding purposes.

1. **Single Neuron sample code**

```
from fractions import Fraction
import numpy as np
import matplotlib.pyplot as plt
import pandas as pd
from scipy.integrate import odeint
import matplotlib as mpl
mpl.rcParams['figure.dpi'] = 300
def alpha_n(V):
    return (0.01*(10.0-V))/(np.exp(1.0-(0.1*V))-1.0)
def beta_n(V):
    return 0.125*np.exp(-V/80.0)
def alpha_m(V):
    return (0.1 * (25.0 - V)) / (np.exp(2.5 - (0.1 * V)) - 1.0)
def beta_m(V):
    return 4.0 * np.exp(-V / 18.0)
def alpha_h(V):
    return 0.07 * np.exp(-V / 20.0)
def beta_h(V):
    return 1.0 / (np.exp(3.0 - (0.1 * V)) + 1.0)
VK = -12.0
VNa = 115.0
Vl = 10.613
gK_mat = np.linspace(5.0,50.0,10)
gNa = 120.0
gL = 0.3
Cm = 1.0
tstart = 0.0
tend = 150.0
timesteps = 10000
T = np.linspace(tstart,tend,timesteps)
def I(t):
    return I_val
def action_potential(x, t):
    dx = np.zeros(4)
    n = x[0]
    m = x[1]
    h = x[2]
    V = x[3]
    dx[0] = alpha_n(V)*(1-n) - beta_n(V)*n
    dx[1] = alpha_m(V)*(1.0-m) - beta_m(V)*m
    dx[2] = alpha_h(V)*(1.0-h) - beta_h(V)*h
    dx[3] = (1/Cm)*(I(t)-(gK*np.power(n,4)*(V-VK))-(gNa*np.power(m,3)*h*(V-VNa))-(gL*(V-Vl)))
    return dx
V0 = np.array([0.0,0.0,0.0,0.0])
%matplotlib inline
count_I_loop = 0
count_gK_loop = 0
for gK in gK_mat:
    for I_val in I_val_mat:
        Vx = odeint(action_potential,V0,T)
        plt.figure()
        plt.plot(T,Vx[:,3])
        plt.title("Current value : {} mA, gK value : {} mS/cm^2".format(I_val,gK))
        plt.xlabel('time in msec')
        plt.ylabel('Voltage (mV)')
        count_I_loop = count_I_loop + 1
    count_gK_loop = count_gK_loop + 1
count_I_loop = 0
count_gK_loop = 0
```

This code was modified from a code given by Giusseppe Bonaccorso. The link is given in the footnote. [1]

2. **Peak counting in action potentials**

```
Vx = odeint(action_potential,V0,T)
plt.figure()
plt.plot(T,Vx[:,3])
plt.title("Neuron - current value : {}".format(I_val))
plt.xlabel('time in msec')
plt.ylabel('Voltage (mV)')
count_peaks = 0
for t in range(int(timesteps/2),timesteps-1):
    if Vx[t,3]>20.0:
        if Vx[t-1,3]>20.0 and Vx[t+1,3]>20.0:
            count_peaks=count_peaks
        else:
            count_peaks=count_peaks+1
print(int(count_peaks/2))
```

3. **Multiple coupled neurons**

The code is similar to that of single neuron except for higher number of output variables for larger number of neurons. The coupling is introduced according to theory given above in the thesis.

4. **Space-Time plot generating script**

```
count_gC_loop = 0
count_I_loop = 0
import numpy as np; np.random.seed(0)
import seaborn as sns; sns.set()
for I_val in I_list:
    for gC_val in gC_list:
        Vx = odeint(neuron1,V0,T)
        plt.figure()
        uniform_data = [Vx[3000:timesteps,3],Vx[3000:timesteps,7],
        Vx[3000:timesteps,11],Vx[3000:timesteps,15],
        Vx[3000:timesteps,19],Vx[3000:timesteps,23],
        Vx[3000:timesteps,27],Vx[3000:timesteps,31],
        Vx[3000:timesteps,35],Vx[3000:timesteps,39]]
        ax = sns.heatmap(uniform_data)
    plt.title("10 neuron bidirectional ring : I = {} mA, gC = {} $mS/cm^2$".format(I_val,gC_val))
    plt.xlabel('Time (in msec)')
    plt.ylabel('Neuron number')
        count_gC_loop = count_gC_loop + 1
    count_I_loop = count_I_loop + 1
count_I_loop = 0
count_gC_loop = 0
```

5. **Calculation Synchronization Order parameter**

```
for I_val in I_list:
    R = []
    for gC_val in gC_list:
        Vx = odeint(neuron1,V0,T)
        onlyV = (Vx[3000:timesteps,3],Vx[3000:timesteps,7],
        Vx[3000:timesteps,11],Vx[3000:timesteps,15],
        Vx[3000:timesteps,19],Vx[3000:timesteps,23],
        Vx[3000:timesteps,27],Vx[3000:timesteps,31],
        Vx[3000:timesteps,35],Vx[3000:timesteps,39])
        onlyV = np.transpose(onlyV)
        num_1stterm = (np.sum((np.sum(onlyV,axis = 1)/len(onlyV[0]))**2))/timesteps
        num_2ndterm = ((np.sum(np.sum(onlyV,axis = 1)/len(onlyV[0])))/timesteps)**2
        num = num_1stterm - num_2ndterm
        num
        den_1stterm = (np.sum(onlyV**2,axis = 0))/timesteps
        den_2ndterm = ((np.sum(onlyV,axis = 0))/timesteps)**2
        den_t = den_1stterm - den_2ndterm
        den = np.sum(den_t)/len(den_t)
        synchronization_par = num/den
        print(synchronization_par)
        R.append(synchronization_par)
```

[1] https://www.bonaccorso.eu/2017/08/19/hodgkin-huxley-spiking-neuron-model-python/

Bibliography

[1] Francisco Bezanilla. Ion channels: from conductance to structure. *Neuron*, 60(3):456–468, 2008.

[2] Wim Van Drongelen. Modeling neural activity. *ISRN Biomathematics*, 2013, 2013.

[3] Alan L Hodgkin and Andrew F Huxley. A quantitative description of membrane current and its application to conduction and excitation in nerve. *The Journal of physiology*, 117(4):500–544, 1952.

[4] RM Rose and JL Hindmarsh. The assembly of ionic currents in a thalamic neuron i. the three-dimensional model. *Proceedings of the Royal Society of London. B. Biological Sciences*, 237(1288):267–288, 1989.

[5] LF Abbott and Thomas B Kepler. Model neurons: from hodgkin-huxley to hopfield. In *Statistical mechanics of neural networks*, pages 5–18. Springer, 1990.

[6] Richard FitzHugh. Impulses and physiological states in theoretical models of nerve membrane. *Biophysical journal*, 1(6):445, 1961.

[7] Jinichi Nagumo, Suguru Arimoto, and Shuji Yoshizawa. An active pulse transmission line simulating nerve axon. *Proceedings of the IRE*, 50(10):2061–2070, 1962.

[8] Anthony N Burkitt. A review of the integrate-and-fire neuron model: I. homogeneous synaptic input. *Biological cybernetics*, 95(1):1–19, 2006.

[9] John Milnor. On the concept of attractor. In *The theory of chaotic attractors*, pages 243–264. Springer, 1985.

[10] Michael G Crandall and Paul H Rabinowitz. Mathematical theory of bifurcation. In *Bifurcation Phenomena in Mathematical Physics and Related Topics*, pages 3–46. Springer, 1980.

[11] Arkady Pikovsky, Jurgen Kurths, Michael Rosenblum, and Jürgen Kurths. *Synchronization: a universal concept in nonlinear sciences*, volume 12. Cambridge university press, 2003.

[12] AS Pikovsky. On the interaction of strange attractors. *Zeitschrift für Physik B Condensed Matter*, 55(2):149–154, 1984.

[13] Louis M Pecora and Thomas L Carroll. Synchronization in chaotic systems. *Physical review letters*, 64(8):821, 1990.

[14] Michael G Rosenblum, Arkady S Pikovsky, and Jürgen Kurths. From phase to lag synchronization in coupled chaotic oscillators. *Physical Review Letters*, 78(22):4193, 1997.

[15] R Herrero, R Pons, J Farjas, F Pi, and G Orriols. Homoclinic dynamics in experimental shil'nikov attractors. *Physical Review E*, 53(6):5627, 1996.

[16] AS Pikovsky, MG Rosenblum, and J Kurths. Synchronization in a population of globally coupled chaotic oscillators. *EPL (Europhysics Letters)*, 34(3):165, 1996.

[17] F Pallasdies, S Goedeke, W Braun, and R Memmesheimer. From single neurons to behavior in the jellyfish aurelia aurita. 2019.

[18] William Ashby. *Design for a brain: The origin of adaptive behaviour*. Springer Science & Business Media, 2013.

[19] Eugene M Izhikevich. *Dynamical systems in neuroscience*. MIT press, 2007.

[20] Henri Korn, Constantino Sotelo, and Francis Crepel. Electrotonic coupling between neurons in the rat lateral vestibular nucleus. *Experimental brain research*, 16(3):255–275, 1973.

[21] Howard J Curtis and David M Travis. Conduction in purkinje tissue of the ox heart. *American Journal of Physiology-Legacy Content*, 165(1):173–178, 1951.

[22] MVL Bennett. Electrical transmission: a functional analysis and comparison to chemical transmission. *Comprehensive Physiology*, pages 357–416, 2011.

[23] Mario Galarreta and Shaul Hestrin. Frequency-dependent synaptic depression and the balance of excitation and inhibition in the neocortex. *Nature neuroscience*, 1(7):587–594, 1998.

[24] Jordi Garcia-Ojalvo, Michael B Elowitz, and Steven H Strogatz. Modeling a synthetic multicellular clock: repressilators coupled by quorum sensing. *Proceedings of the National Academy of Sciences*, 101(30):10955–10960, 2004.

[25] S Rajesh, Sudeshna Sinha, and Somdata Sinha. Synchronization in coupled cells with activator-inhibitor pathways. *Physical Review E*, 75(1):011906, 2007.

[26] A Aldo Faisal, Luc PJ Selen, and Daniel M Wolpert. Noise in the nervous system. *Nature reviews neuroscience*, 9(4):292–303, 2008.

[27] Jerzy Neyman. Frequentist probability and frequentist statistics. *Synthese*, pages 97–131, 1977.

[28] Bruno A Olshausen. Bayesian probability theory. *The Redwood Center for Theoretical Neuroscience, Helen Wills Neuroscience Institute at the University of California at Berkeley, Berkeley, CA*, 2004.

[29] John Hammersley. *Monte carlo methods*. Springer Science & Business Media, 2013.

[30] Don Van Ravenzwaaij, Pete Cassey, and Scott D Brown. A simple introduction to markov chain monte–carlo sampling. *Psychonomic bulletin & review*, 25(1):143–154, 2018.

[31] Nicholas Metropolis, Arianna W Rosenbluth, Marshall N Rosenbluth, Augusta H Teller, and Edward Teller. Equation of state calculations by fast computing machines. *The journal of chemical physics*, 21(6):1087–1092, 1953.

[32] W Keith Hastings. Monte carlo sampling methods using markov chains and their applications. 1970.

[33] Simon Duane, Anthony D Kennedy, Brian J Pendleton, and Duncan Roweth. Hybrid monte carlo. *Physics letters B*, 195(2):216–222, 1987.

[34] Alan E Gelfand and Adrian FM Smith. Sampling-based approaches to calculating marginal densities. *Journal of the American statistical association*, 85(410):398–409, 1990.

[35] SA Sisson, Y Fan, and MA Beaumont. Overview of abc. *Handbook of approximate Bayesian computation*, pages 3–54, 2018.

[36] J Andrew Doyle and Alan C Evans. What colour is neural noise? *arXiv preprint arXiv:1806.03704*, 2018.

[37] Mikhail I Rabinovich, Pablo Varona, Allen I Selverston, and Henry DI Abarbanel. Dynamical principles in neuroscience. *Reviews of modern physics*, 78(4):1213, 2006.

[38] Misha Rabinovich, Ramon Huerta, and Gilles Laurent. Transient dynamics for neural processing. *Science*, 321(5885):48–50, 2008.

[39] Luigi De Gennaro and Michele Ferrara. Sleep spindles: an overview, 2003.